Heavy quasiparticle bands in the underscreened quasiquartet Kondo lattice

Peter Thalmeier[1] and Alireza Akbari[2,3,4]

[1]*Max Planck Institute for the Chemical Physics of Solids, D-01187 Dresden, Germany*
[2]*Asia Pacific Center for Theoretical Physics, Pohang, Gyeongbuk 790-784, Korea*
[3]*Department of Physics, POSTECH, Pohang, Gyeongbuk 790-784, Korea*
[4]*Max Planck POSTECH Center for Complex Phase Materials, POSTECH, Pohang 790-784, Korea*

(Received 1 August 2018; revised manuscript received 19 September 2018; published 11 October 2018)

We study the quasiparticle spectrum in an underscreened Kondo-lattice (KL) model that involves a single spin degenerate conduction band and two crystalline-electric-field (CEF) split Kramers doublets coupled by both orbital-diagonal and nondiagonal exchange interactions. We find the three quasiparticle bands of the model using a constrained fermionic mean field approach. While two bands are similar to the one-orbital model, a new genuinely heavy band inside the main hybridization gap appears in the quasiquartet model. Its dispersion is due to effective hybridization with conduction states, but the bandwidth is controlled by the size of the CEF splitting. Furthermore, several new indirect and direct hybridization gaps may be identified. By solving the self-consistency equation, we calculate the CEF splitting and exchange dependence of effective Kondo low-energy scale, hybridization gaps, and bandwidths. We also derive the quasiparticle spectral densities and their partial orbital contributions. We suggest that the two-orbital KL model can exhibit mixed CEF/Kondo excitonic magnetism.

DOI: 10.1103/PhysRevB.98.155121

I. INTRODUCTION

The Anderson lattice and Kondo lattice (KL) models provide the basic understanding for strongly correlated f-electron systems like heavy-fermion metals, superconductors, and Kondo insulators [1–5]. In the KL model, the charge fluctuations between conduction and f electrons are already eliminated leading to conduction electrons that interact through an effective Schrieffer-Wolff exchange term with a lattice of localized moments resulting from the total angular momentum $\mathbf{J}$ of the f-electron shell. Their $(2J+1)$-fold state degeneracy is reduced by the action of the crystalline electric field leaving (for noninteger J) only twofold-degenerate (e.g., for common tetragonal symmetry D_{4h}) Kramers doublets or at the most fourfold-degenerate quartets (in cubic symmetry O_h) as in Ce- [6,7] or Sm-hexaboride [8] Kondo compounds.

In Kondo lattice studies it is frequently assumed that the degeneracy of conduction states is the same as that of localized states, leading to a SU(N) internal symmetry of the KL Hamiltonian. This is reasonable for the $N=2$ degeneracy of a doublet ground state because of the Kramers degeneracy of conduction electrons when inversion and time-reversal symmetry are preserved. However, fourfold degeneracy of conduction states may only appear along symmetry lines or possibly symmetry planes, but generally not throughout the whole Brillouin zone. Therefore, for $N>2$ this model is rather artificial. It is nevertheless useful because it is accessible to a simple constrained mean field approach which becomes exact in the large-N degeneracy limit [1,9]. This leads very naturally to hybridized itinerant bands with partly heavy f character that are described by the simple dispersions $E_{1,2\mathbf{k}} = \frac{1}{2}(\epsilon_{\mathbf{k}}+\lambda) \pm \frac{1}{2}\sqrt{(\epsilon_{\mathbf{k}}-\lambda)^2+4\bar{V}^2}$ where $\lambda, \bar{V}$ are self-consistently determined effective f-level position and hybridization, respectively, the former defining the low-energy Kondo scale of the system. In the original Anderson model, one generally may also have a $\mathbf{k}$-dependent hybridization $\bar{V}_{\mathbf{k}}$ with nodes leading to pseudogap behavior [10,11]. Most of the qualitative understanding of heavy band and hybridization gap formation and its physical consequences is based on this simple result for the equal degeneracy or "fully screened" model. This designation stems from the corresponding impurity model where the local f moment will be fully screened at low temperature by the exchange with conduction electrons leading to just an enhanced Pauli susceptibility. However, even in the fully screened case ($N=2$), many Kondo compounds become magnetically ordered [12], which is commonly explained as a rigid heavy band polarization [13–16] in the lattice model. The type of magnetic order then depends on the filling of conduction band and strength of Kondo coupling. A more advanced dynamical mean field theory (DMFT) approach to KL magnetism beyond the rigid band model is used in Refs. [17,18].

For application to realistic Kondo systems, in particular Ce and Yb compounds, the SU(2) model seems oversimplified. In the case of cubic compounds, the ground state may be a quartet, then more than one hybridization gap may appear, e.g., in cubic YbB_{12} [19] or more complicated order than magnetic is observed as, e.g., in cubic CeB_6 [20]. Even in tetragonal systems, in particular in Yb compounds, the projection to the SU(2) model for the lowest Kramers doublet is too restrictive because of a close by first excited CEF Kramers state, forming a quasiquartet with the ground state. This case is, e.g., realized in $YbRu_2Ge_2$ [21–23] and other Yb and Ce compounds [24,25] with $\Gamma_6-\Gamma_7$ low-lying quasiquartet. This opens a new possibility, namely, induced or excitonic magnetic or

even multipolar order due to orbitally nondiagonal exchange couplings [22].

This extension should also have profound consequences for the Kondo physics. First, the inclusion of the excited state implies that we have an underscreening situation with total number of $2N$ f states and $N = 2$ for the conduction band degeneracy which can drastically change the spectral properties of hybridized bands [26]. Second, the CEF splitting should strongly influence the Kondo energy scale which becomes dependent on the splitting size, as is well known in the impurity models [27] and also on the difference in diagonal and the additional off-diagonal exchange couplings. A most interesting aspect is the influence of (partial) Kondo screening on the possible excitonic order in the two-orbital quasiquartet KL. This requires first a thorough understanding of how the localized split CEF states turn into quasiparticle bands due to the Kondo effect. So far, the underscreened KL has been less extensively investigated. Existing work [28–30] discusses possible magnetic phases and the ground-state phase diagram without emphasis on CEF effects. In this work, we perform a detailed study of a two-orbital underscreened KL model with quasiquartet CEF states, in particular, in view of its quasiparticle dispersion, hybridization gaps, CEF-splitting-dependent Kondo energy scale, and spectral properties. This is a prerequisite for discussing physical applications like induced (excitonic) magnetism or multipolar order and possible spin exciton modes in the paramagnetic phase as well as the broken symmetry phases for such a more realistic Kondo lattice model.

The paper is organized as follows: In Sec. II we introduce the quasiquartet KL model and its fermionic representation. The treatment within constrained mean field theory for the strongly correlated f-electron limit is presented in Sec. III. Then, in Sec. IV the quasiparticle bands are derived and their properties like bandwidths, effective mass, and hybridization gaps are discussed. Section V introduces the Green's functions of the model that give the basis for formulating the self-consistency requirements and constraints in Sec. VI. The numerical solutions, in particular spectral properties, are discussed in Sec. VII and, finally, Sec. VIII gives the conclusions and outlook on further applications of the model.

II. MODEL OF THE QUASIQUARTET KONDO LATTICE

We investigate the Kondo-lattice (KL) model for a quasiquartet system of $4f$-CEF states, having in mind $Yb^{3+}(4f^{13})$ or $Ce^{3+}(4f^1)$ Kondo ions with one f hole or electron, respectively. The doublet constituents of this model CEF scheme split by an energy $\Delta_0 = 2\Delta$ are treated as Kramers $S = \frac{1}{2}$ pseudospins. It is sketched in Fig. 1 and its exchange interactions with conduction (c) electrons are indicated. A more detailed discussion based on Ref. [22] is given in Appendix A. The effect of c-f hybridization and f-f Coulomb interaction is described by the Anderson lattice model [2]. The Coulomb interaction is the largest energy scale and may be eliminated by a Schrieffer-Wolff transformation [31]. This leads to a Kondo-type Hamiltonian with effective antiferromagnetic (AF) exchange of strength $(g_J - 1)I_{ex}$ between the conduction electron spins and the localized $4f$ moments which (partly) screen them at low temperature. We consider a

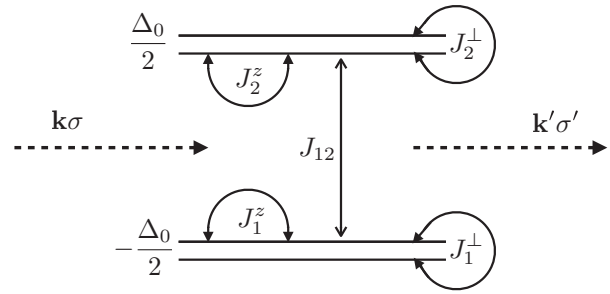

FIG. 1. Sketch of the quasiquartet CEF level scheme consisting of two Kramers doublets ($\tau = 1, 2$ CEF orbital index, e.g., for Γ_6, Γ_7) with splitting Δ_0. The various diagonal ($J_\tau^\perp$, J_τ^z) and off-diagonal (J_{12}) interactions are indicated which scatter conduction electrons from state ($\mathbf{k}\sigma$) to ($\mathbf{k}'\sigma'$).

model with only *one* conduction band but *two* pseudospins representing the two lowest $4f$ Kramers doublets of the $(2J + 1)$ CEF scheme. Therefore, the degeneracy of conduction states is $N = 2$ whereas there are $2N = 4$ localized quasiquartet states. In the impurity case with just one f site, such model is termed "underscreened" [28,32] because in this case (for $\Delta_0 = 0$) the local $4f$ moment cannot be fully screened to form a singlet ground state so that a residual spin $S^* = \frac{1}{2}$ survives, leading to a Curie-type susceptibility contribution at low temperature. Nevertheless, the Kondo fixed point and associated local Fermi liquid is stable in the underscreened case because the residual FM coupling of S^* to the renormalized conduction states scales logarithmically to zero [32,33]. This is in contrast to the overscreened case (more than N conduction channels) where the Kondo fixed point is unstable leading to non-Fermi-liquid behavior. While the impurity case is understood there are few treatments for the underscreened quasiquartet Kondo lattice model, which is, however, of some practical importance in tetragonal (D_{4h} symmetry) Ce and Yb compounds. The model is defined by the Hamiltonian

$$H = H_0 + (g_J - 1)I_{ex} \sum_i \mathbf{s}_i \cdot \mathbf{J}_i, \tag{1}$$

where g_J is the Landé factor of the lowest total angular momentum ($\mathbf{J}$) state of $Ce^{3+}(4f^1,\ J = \frac{5}{2})$ electron or $Yb^{3+}(4f^{13},\ J = \frac{7}{2})$ hole and $\mathbf{s}$ the conduction electron spin. The first part of the Hamiltonian describes noninteracting conduction electrons and CEF states. When we restrict the latter to the two lowest Kramers doublet states in Fig. 1, one may transform it to a fermionic representation as described in Appendix A according to

$$\begin{aligned}
H &= H_0 + H_{cf} + H_{cf}^{(12)},\\
H_0 &= \sum_{\mathbf{k}\sigma} \epsilon_{\mathbf{k}} c_{\mathbf{k}\sigma}^\dagger c_{\mathbf{k}\sigma} + \frac{1}{2}\Delta_0 \sum_{i\tau\sigma} (-1)^\tau f_{i\tau\sigma}^\dagger f_{i\tau\sigma},\\
H_{cf} &= \frac{1}{4}\sum_{i\tau} J_\tau^z (f_{i\tau\uparrow}^\dagger f_{i\tau\uparrow} - f_{i\tau\downarrow}^\dagger f_{i\tau\downarrow})(c_{i\tau\uparrow}^\dagger c_{i\tau\uparrow} - c_{i\tau\downarrow}^\dagger c_{i\tau\downarrow})\\
&\quad + \frac{1}{2}\sum_{i\tau} J_\tau^\perp (f_{i\tau\uparrow}^\dagger f_{i\tau\downarrow} c_{i\downarrow}^\downarrow c_{i\uparrow} + f_{i\tau\downarrow}^\dagger f_{i\tau\uparrow} c_{i\uparrow}^\dagger c_{i\downarrow}),\\
H_{cf}^{(12)} &= \frac{1}{2} J_{12} \sum_{i\tau} (f_{i\tau\downarrow}^\dagger f_{i\bar{\tau}\uparrow} c_{i\uparrow}^\downarrow c_{i\downarrow} + f_{i\tau\uparrow}^\dagger f_{i\bar{\tau}\downarrow} c_{i\downarrow}^\downarrow c_{i\uparrow}).
\end{aligned} \tag{2}$$

Here, $c^\dagger_{\mathbf{k}\sigma}$ create the single-band conduction states with dispersion denoted by $\epsilon_{\mathbf{k}}$ and spin degeneracy by $\sigma = \uparrow, \downarrow$, respectively. The second term in H_0 describes the $4f$ quasiquartet of Fig. 1 with the two constituent Kramers doublets at lattice sites $\mathbf{R}_i$ and with pseudospin index $\sigma = \uparrow, \downarrow$. The doublets are denoted by the orbital index $\tau = 1, 2$ (lower and upper doublets, respectively). The second term H_{cf} corresponds to *elastic* exchange scattering of c electrons from each doublet while the third term $H^{(12)}_{cf}$ is associated with the *inelastic* (off-diagonal) scattering between the orbitally different doublets. Due to tetragonal symmetry, the former is described by sets of constants J^z_τ, $J^\perp_\tau$ ($\tau = 1, 2$) for exchange parallel and perpendicular to the tetragonal z axis. For the inelastic term, $J^z_{12} = 0$ and we define $J_{12} \equiv J^\perp_{12}$ (for details see Appendix A). In this work, we restrict to the case where all effective couplings are antiferromagnetic, although more general cases are possible (Appendix A). Furthermore, we investigate only the paramagnetic phase within the constrained mean field approach. Then, only the set of three transverse exchange parameters $J^\perp_\tau$, J_{12} contribute to the ground-state energy and quasiparticle energies within mean field decoupling scheme [1,9] of H carried out in the following section.

III. CONSTRAINED MEAN FIELD THEORY

For this purpose, we introduce as (nonmagnetic) order parameter the effective homogeneous hybridization field generalized from Refs. [1,9] or Refs. [13–16] and defined by

$$V_\tau = \langle \hat{V}_{i\tau} \rangle = \langle f^\dagger_{i\tau\downarrow} c_{i\downarrow} + c^\dagger_{i\uparrow} f_{i\tau\uparrow} \rangle,$$
$$V_{\tau\bar{\tau}} = \langle \hat{V}_{i\tau\bar{\tau}} \rangle = \langle f^\dagger_{i\tau\downarrow} c_{i\downarrow} + c^\dagger_{i\uparrow} f_{i\bar{\tau}\uparrow} \rangle. \tag{3}$$

We set the gauge to $V_\tau = V^*_\tau$ and $V_{\tau\bar{\tau}} = V^*_{\tau\bar{\tau}}$ and restrict to the symmetric case $V_{\tau\bar{\tau}} = V_{\bar{\tau}\tau}$. It is easy to show that $V_{12} = V_{21} = \frac{1}{2}(V_1 + V_2)$. Here, V_τ describes the amplitude of each f doublet to form a singlet state with a conduction electron at the same site.

The effect of large f-f Coulomb interaction is to exclude doubly occupied states for electrons (holes) in the f-electron Hilbert space. This may be achieved by adding a Lagrange term according to

$$H^\lambda = H + \sum_i \lambda_i \left(\sum_\tau \hat{n}^f_{i\tau} - 1 \right), \quad \hat{n}^f_{i\tau} = \sum_\sigma f^\dagger_{i\tau\sigma} f_{i\tau\sigma}. \tag{4}$$

The constraint of single f occupancy is enforced only globally in the mean field approach. Using Eq. (3), the decoupling leads to

$$\begin{aligned} H^\lambda_{mf} &= E^\lambda_0 + \tilde{H}^\lambda_{mf} \\ &= E^\lambda_0 + \sum_{\mathbf{k}\sigma} \epsilon_{\mathbf{k}} c^\dagger_{\mathbf{k}\sigma} c_{\mathbf{k}\sigma} + \sum_{\mathbf{k}\tau\sigma} \epsilon^\lambda_{0\tau} f^\dagger_{\mathbf{k}\tau\sigma} f_{\mathbf{k}\tau\sigma} \\ &\quad + \sum_{\mathbf{k}\tau\sigma} \bar{V}_\tau (f^\dagger_{\mathbf{k}\tau\sigma} c_{\mathbf{k}\sigma} + c^\dagger_{\mathbf{k}\sigma} f_{\mathbf{k}\tau\sigma}). \end{aligned} \tag{5}$$

Here, we defined

$$E^\lambda_0 = \frac{1}{2} \sum_\tau J^\perp_\tau V^2_\tau + J_{12} V^2_{12} - \lambda, \quad \epsilon^\lambda_{0\tau} = \lambda + (-1)^\tau \frac{\Delta_0}{2}, \tag{6}$$

furthermore, we introduced the mixed hybridization amplitudes given by

$$\begin{pmatrix} \bar{V}_1 \\ \bar{V}_2 \end{pmatrix} = -\frac{1}{2} \begin{pmatrix} J^\perp_1 + \frac{1}{2} J_{12} & \frac{1}{2} J_{12} \\ \frac{1}{2} J_{12} & J^\perp_2 + \frac{1}{2} J_{12} \end{pmatrix} \begin{pmatrix} V_1 \\ V_2 \end{pmatrix}. \tag{7}$$

This transformation expresses the influence of nondiagonal (inelastic) exchange terms in the singlet formation.

The total ground-state energy (per site, N_s = number of sites) is then given by

$$\begin{aligned} E^\lambda_{gs}/N_s &= \langle H^\lambda_{mf} \rangle / N_s \\ &= \frac{1}{N_s} \sum_{\mathbf{k}\sigma} \epsilon_{\mathbf{k}} n^c_{\mathbf{k}\sigma} + \frac{1}{2} \Delta_0 (n^f_2 - n^f_1) \\ &\quad + \lambda (n^f_1 + n^f_2 - 1) + \frac{1}{2} (J^\perp_1 V^2_1 + J^\perp_2 V^2_2) + J_{12} V^2_{12} \\ &\quad - \frac{1}{2} \sum_\tau (J^\perp_\tau V_\tau + J_{12} V_{12}) \frac{2}{N_s} \sum_{\mathbf{k}\sigma} \langle f^\dagger_{\mathbf{k}\tau\sigma} c_{\mathbf{k}\sigma} \rangle, \end{aligned} \tag{8}$$

where we defined

$$n^c_{\mathbf{k}\sigma} = \langle c^\dagger_{\mathbf{k}\sigma} c_{\mathbf{k}\sigma} \rangle, \quad n^f_\tau = \sum_\sigma \langle f^\dagger_{i\tau\sigma} f_{i\tau\sigma} \rangle, \tag{9}$$

as the c- and f-electron occupations, respectively. For noninteracting conduction electrons we have $n^c_{\mathbf{k}\sigma} = \Theta_H(\mu - \epsilon_{\mathbf{k}\sigma})$, where μ is the chemical potential and Θ_H the Heaviside function.

Minimization of the ground-state energy with respect to λ and V_τ leads to

$$\begin{aligned} n_f &= n^f_1 + n^f_2 = 1, \\ V_\tau &= \frac{1}{N_s} \sum_{\mathbf{k}\sigma} \langle f^\dagger_{\mathbf{k}\tau\sigma} c_{\mathbf{k}\sigma} \rangle, \end{aligned} \tag{10}$$

which express single occupancy constraint and hybridization self-consistency, respectively. Furthermore, minimization with respect to V_{12} only gives $V_{12} = \frac{1}{2}(V_1 + V_2)$ consistent with the definitions in Eq. (3). Then, introducing the spinors $\Psi^\dagger_{\mathbf{k}\sigma} = (c^\dagger_{\mathbf{k}\sigma}, f^\dagger_{1\mathbf{k}\sigma}, f^\dagger_{2\mathbf{k}\sigma})$ we obtain the bilinear mean field Hamiltonian given by

$$\tilde{H}^\lambda_{mf} = \sum_{\mathbf{k}m} \Psi^\dagger_{\mathbf{k}m} \hat{h}_{\mathbf{k}} \Psi_{\mathbf{k}m}, \quad \hat{h}_{\mathbf{k}} = \begin{pmatrix} \epsilon_{\mathbf{k}} & \bar{V}_1 & \bar{V}_2 \\ \bar{V}_1 & \epsilon^\lambda_{01} & 0 \\ \bar{V}_2 & 0 & \epsilon^\lambda_{02} \end{pmatrix}. \tag{11}$$

We abbreviate $\Delta = \frac{1}{2}\Delta_0$ so that the effective f-level energies are $\epsilon^\lambda_{01} = \lambda - \Delta$, $\epsilon^\lambda_{02} = \lambda + \Delta$. Furthermore, $\epsilon^\lambda_{\mathbf{k}} = \epsilon_{\mathbf{k}} - \lambda$ will be used.

IV. QUASIPARTICLE BANDS AND STATES

In this section, we discuss the basic properties like dispersions, wave functions, hybridization gaps, and effective masses of the quasiparticle bands which may be found in closed form from diagonalizing the above bilinear mean field Hamiltonian.

A. Hybridized dispersions and wave functions

The hybridized quasiparticle dispersions are obtained by finding the zeros of the characteristic polynomial of $\hat{h}_{\mathbf{k}}$ given

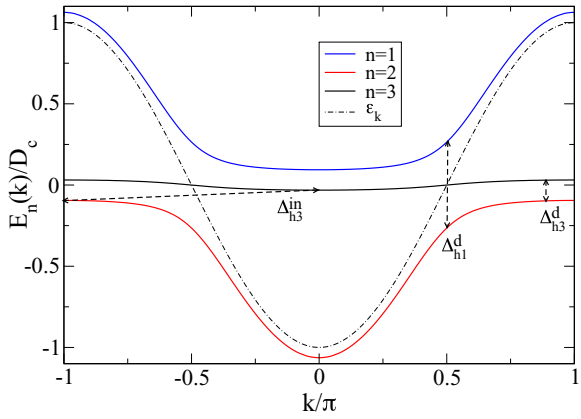

FIG. 2. Hybridized quasiparticle bands $E_{n\mathbf{k}}$ (a) along straight BZ path $M(-\pi,-\pi)-\Gamma(0,0)-M(\pi,\pi)$ with some direct and indirect hybridization gaps indicated (Sec. IV B). There are *two* different direct hybridization gaps in the two-orbital KL model. The larger (Δ^d_{h1}) is determined by the effective hybridization scale $\bar{V}$, the smaller (Δ^d_{h3}) by the Kondo scale T^*. The latter is of the same size as the indirect gap Δ^{in}_{h3}. Parameters are $J_1^\perp = 0.470$, $J_2^\perp = 0.767$, $J_{12} = 0.2$, $\Delta = 0.056$. Then, the particle-hole-symmetric case is realized with self-consistently determined $\bar{V}_1 = \bar{V}_2 = 0.183$ and setting $\mu = -0.096$ (top of band $n = 2$). All energies in this and subsequent figures are given in units of the half-conduction band with D_c.

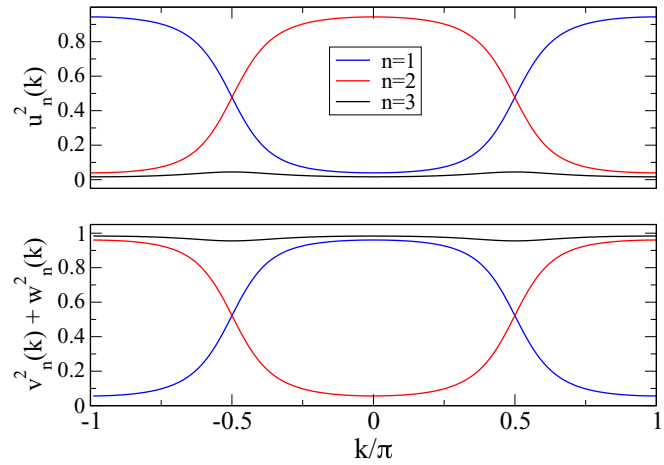

FIG. 3. Weights for c electrons (top) and total f-electron weight (bottom) for hybridized quasiparticle bands along [11] M-Γ-M direction (cf. Fig. 2). For the central heavy band ($n = 3$) conduction state weight $u_3^2(\mathbf{k})$ is small and total f weight $v_3^2(\mathbf{k}) + w_3^2(\mathbf{k})$ is close to one. For the upper ($n = 1$) and lower ($n = 2$) hybridized bands, these weights alternate over the BZ.

by $d_{\mathbf{k}}(i\omega_n) = \det(i\omega_n - \hat{h})$ (ω_n is a Matsubara frequency). Its evaluation leads to

$$\begin{aligned} d_{\mathbf{k}}(i\omega_n) &= (i\omega_n - \epsilon_{\mathbf{k}})\big(i\omega_n - \epsilon^\lambda_{01}\big)\big(i\omega_n - \epsilon^\lambda_{02}\big) \\ &\quad - \bar{V}_1^2\big(i\omega_n - \epsilon^\lambda_{02}\big) - \bar{V}_2^2\big(i\omega_n - \epsilon^\lambda_{01}\big) \\ &= (i\omega_n - E_{1\mathbf{k}})(i\omega_n - E_{2\mathbf{k}})(i\omega_n - E_{3\mathbf{k}}). \end{aligned} \tag{12}$$

The three hybridized quasiparticle bands $E_{n\mathbf{k}}$ ($n = 1, 2, 3$) are obtained from solving $d_{\mathbf{k}}(i\omega_n) = 0$ as

$$\begin{aligned} E_{1\mathbf{k}} &= \lambda + \frac{1}{3}\epsilon^\lambda_{\mathbf{k}} + 2\sqrt[3]{r_{\mathbf{k}}}\cos\left(\frac{\phi_{\mathbf{k}}}{3}\right), \\ E_{2\mathbf{k}} &= \lambda + \frac{1}{3}\epsilon^\lambda_{\mathbf{k}} + 2\sqrt[3]{r_{\mathbf{k}}}\cos\left(\frac{\phi_{\mathbf{k}}}{3} + \frac{2\pi}{3}\right), \\ E_{3\mathbf{k}} &= \lambda + \frac{1}{3}\epsilon^\lambda_{\mathbf{k}} + 2\sqrt[3]{r_{\mathbf{k}}}\cos\left(\frac{\phi_{\mathbf{k}}}{3} + \frac{4\pi}{3}\right). \end{aligned} \tag{13}$$

These relations generalize the simple one f-orbital hybridization formula mentioned in the Introduction to the case of a CEF split two-orbital system. Here, the auxiliary functions $r_{\mathbf{k}}$, $\phi_{\mathbf{k}}$ are given by

$$\begin{aligned} r_{\mathbf{k}} &= \left(\frac{1}{3}\left[(\Delta^2 + \bar{V}^2) + \frac{1}{3}\epsilon^{\lambda 2}_{\mathbf{k}}\right]\right)^{\frac{3}{2}}, \\ \cos\phi_{\mathbf{k}} &= \frac{1}{2r_{\mathbf{k}}}\left\{\frac{1}{3}\epsilon^\lambda_{\mathbf{k}}\left[\frac{2}{9}\epsilon^{\lambda 2}_{\mathbf{k}} + (\Delta^2 + \bar{V}^2)\right] - \Delta\big(\epsilon^\lambda_{\mathbf{k}}\Delta + \delta_s\big)\right\}, \end{aligned} \tag{14}$$

where we defined $\bar{V}^2 = \bar{V}_1^2 + \bar{V}_2^2$ and $\delta_s = \bar{V}_1^2 - \bar{V}_2^2$. The three quasiparticle bands $E_{n\mathbf{k}}$ are shown in Fig. 2 for a special parameter set with $\bar{V}_\tau$ evaluated self-consistently as described in Sec. VI. For this figure [and the associated density of states (DOS) in Fig. 5] we use parameters such that particle-hole symmetry is preserved. There is a distinctive difference to the fully screened KL model (one orbital per conduction band): In the latter, one has only an upper and a lower hybridized band similar to bands $n = 1, 2$ in Fig. 2 with $E_{3\mathbf{k}}$ missing. In the present underscreened model with two f orbitals, there is a third narrow band $E_{3\mathbf{k}}$ within the large direct hybridization gap Δ^d_{h1} in Fig. 2. Thus, the present model provides the existence of a heavy band extending throughout the Brillouin zone (BZ), contrary to the single f-orbital model where the heavy mass appears only on the zone center and boundary alternatively for the two bands.

In addition to the dispersion, it is important to know the composition of Bloch states in terms of conduction and localized f states for all wave vectors according to

$$\big|\Psi^n_{\mathbf{k}\sigma}\big\rangle = u^n_{\mathbf{k}} c^\dagger_{\mathbf{k}\sigma}|0\rangle + v^n_{\mathbf{k}} f^\dagger_{1\mathbf{k}\sigma}|0\rangle + w^n_{\mathbf{k}} f^\dagger_{2\mathbf{k}\sigma}|0\rangle, \tag{15}$$

where $n = 1$–3 is the band index denoting band $E_{n\mathbf{k}}$ and associated Bloch state $|\Psi^n_{\mathbf{k}\sigma}\rangle$. For these eigenstates of $\hat{h}_{\mathbf{k}}$ we obtain

$$\begin{aligned} u^{n2}_{\mathbf{k}} &= \big[\bar{V}_1^2\big(E_{n\mathbf{k}} - \epsilon^\lambda_{02}\big) + \bar{V}_2^2\big(E_{n\mathbf{k}} - \epsilon^\lambda_{01}\big)\big]^2 / D^n_{\mathbf{k}}, \\ v^{n2}_{\mathbf{k}} &= \bar{V}_1^2\big(E_{n\mathbf{k}} - \epsilon^\lambda_{02}\big)^2 (E_{n\mathbf{k}} - \epsilon_{\mathbf{k}})^2 / D^n_{\mathbf{k}}, \\ w^{n2}_{\mathbf{k}} &= \bar{V}_2^2\big(E_{n\mathbf{k}} - \epsilon^\lambda_{01}\big)^2 (E_{n\mathbf{k}} - \epsilon_{\mathbf{k}})^2 / D^n_{\mathbf{k}}, \end{aligned} \tag{16}$$

and

$$\begin{aligned} D^n_{\mathbf{k}} &= (E_{n\mathbf{k}} - \epsilon_{\mathbf{k}})^2\big[\bar{V}_1^2\big(E_{n\mathbf{k}} - \epsilon^\lambda_{02}\big)^2 + \bar{V}_2^2\big(E_{n\mathbf{k}} - \epsilon^\lambda_{01}\big)^2\big] \\ &\quad + \big[\bar{V}_1^2\big(E_{n\mathbf{k}} - \epsilon^\lambda_{02}\big) + \bar{V}_2^2\big(E_{n\mathbf{k}} - \epsilon^\lambda_{01}\big)\big]^2. \end{aligned}$$

These coefficients fulfill the normalization condition $u^{n2}_{\mathbf{k}} + v^{n2}_{\mathbf{k}} + w^{n2}_{\mathbf{k}} = 1$. The c-electron weight $u^2_{n\mathbf{k}}$ and total f weight $v^{n2}_{\mathbf{k}} + w^{n2}_{\mathbf{k}}$ for the three bands are shown in Fig. 3. We note that the bands $n = 1, 2$ have partly c or f character which changes when $\mathbf{k}$ moves across the BZ. (cf. Fig. 2). On the other hand,

the central narrow (heavy) band has predominantly f-electron character throughout the BZ. Its small dispersion is due to a small c-electron admixture.

B. Bandwidths, hybridization gaps, and effective masses

Before we solve the central self-consistency problem for the order parameters $\bar{V}_\tau$ (or V_τ), we assume that they are already known and then discuss certain characteristic features of the quasiparticle bands like widths and hybridization gaps. For this purpose, to keep algebraic expressions simple, we restrict mostly to the symmetric case $\bar{V}_1 = \bar{V}_2 \equiv \bar{V}$ with $\delta_s = 0$ where the spectrum may show particle-hole symmetry for proper choice of μ such that $\lambda = 0$. The condition for its realization and also the asymmetric situation $\bar{V}_1 \neq \bar{V}_2$ will be discussed further in Sec. VII using the numerical results.

We first recall the two hybridized bands $E_{1,2\mathbf{k}}$ in the one f-orbital KL model given in the Introduction. The essential nontrivial features of this model are (i) a direct hybrization gap $\Delta_h^d = 2\bar{V}$ resulting from the anticrossing of conduction band and renormalized f level, (ii) a much smaller indirect hybridization gap $\Delta_h^{in} = 2\frac{\bar{V}^2}{D_c} \ll \Delta_h^d$ which defines a new low-energy scale $T^* = \bar{V}^2/D_c$ that is exponentially small compared to the conduction bandwidth $2D_c$ (see also Appendix B). The fermionic quasiparticle picture of the KL is valid for temperatures much below the characteristic temperature T^*. The low-energy scale is associated with very flat bands near the BZ center and boundaries. The corresponding Bloch states have high effective masses of the order $m^*/m_c \simeq D_c/T^* \gg 1$ (m_c is the bare conduction band mass). The heavy mass quasiparticles and small (indirect) hybridization gap govern the low-temperature ($T \ll T^*$) thermodynamic, transport, and dynamical physical properties of heavy-fermion metals and Kondo semiconductors [2,5,31].

In the underscreened two-f-orbital model this simple picture has to be extended due to the appearance of an additional heavy (narrow) band within the main hybridization gap (Fig. 2). The excitation spectrum may now be characterized by the following bandwidths W_n and hybridization gaps Δ_h^d, Δ_h^{in} which are energy differences of the three bands $E_{n\mathbf{k}}$ at symmetry $\mathbf{k}$ points, e.g., $\mathbf{k} = 0$, $\mathbf{Q}' = (\pi/2, \pi/2)$, and $\mathbf{Q} = (\pi, \pi)$. From Table I we get ($\lambda \ll D_c$) the following Bandwidths:

$$
\begin{aligned}
W_{n=1,2} &= E_{n\mathbf{Q}} - E_{n0} \\
&= D_c + \frac{1}{2}\left(\frac{\bar{V}^2}{D_c} + \frac{\Delta^2}{D_c}\right) - \frac{1}{2}D_c\left[\left(\frac{\bar{V}^2}{D_c^2}\right)^2 + \frac{\Delta_0^2}{D_c^2}\right]^{\frac{1}{2}}, \\
W_3 &= E_{3\mathbf{Q}} - E_{30} \\
&= -\left(\frac{\bar{V}^2}{D_c} + \frac{\Delta^2}{D_c}\right) + D_c\left[\left(\frac{\bar{V}^2}{D_c^2}\right)^2 + \frac{\Delta_0^2}{D_c^2}\right]^{\frac{1}{2}}.
\end{aligned}
$$

Here, for convenience we used both Δ_0 and $\Delta = \frac{\Delta_0}{2}$. For orbital splitting $\Delta_0 \to 0$ we have $W_{n=1,2} \to D_c$ and $W_3 \to 0$. The overall bandwidth of $E_{n=1,2\mathbf{k}}$ bands is little affected by Δ (as is obvious from Fig. 2), it is always of order D_c. On the other hand, the width of the narrow central band $E_{3\mathbf{k}}$ depends sensitively on the orbital splitting Δ_0. For a finite dispersion of $E_{3\mathbf{k}}$, a finite splitting Δ_0 as well as a finite hybridization $\bar{V}$ is required. The Δ dependence of W_3 is shown in Fig. 4 (full black line). This genuinely heavy band is a unique aspect of the quasiquartet KL model. In fact, it directly characterizes the low-energy scale because W_3 may be written as ($T^* = \bar{V}^2/D_c$)

$$
\begin{aligned}
W_3 &= -T^* + \left(T^{*2} + \Delta_0^2\right)^{\frac{1}{2}} \\
&\simeq \begin{cases} \frac{1}{2}\Delta_0\left(\frac{\Delta_0}{T^*}\right), & \Delta_0 < T^* \\ \Delta_0\left[1 - \left(\frac{T^*}{\Delta_0}\right)\right], & \Delta_0 > T^* \end{cases}
\end{aligned} \tag{17}
$$

where we neglected terms of order (Δ^2/D_c). As shown in Fig. 4 the orbital splitting Δ_0 must be finite to get a dispersive central band in Fig. 2. For finite Δ_0 when $T^* \to 0$ the central band degenerates into two flat subbands an energy Δ_0 apart.

From Fig. 2 we also conclude that the band structure of the quasiquartet model KL exhibits several hybridization gaps, in contrast to the single-orbital model: three direct gaps Δ_{hi}^d and three indirect gaps Δ_{hi}^{in} (i = 1–3). For each class, two are equivalent for the symmetric case when $\bar{V}_1 = \bar{V}_2$ and spectral symmetry holds. We then obtain the following

TABLE I. Typical boundary cutoff values of the hybridized bands (Fig. 2) and associated DOS functions in Fig. 5(a). Here, $\bar{V}^2 = \bar{V}_1^2 + \bar{V}_2^2$, $\delta_s = \bar{V}_1^2 - \bar{V}_2^2$. In the last column, terms of order $\approx(\Delta^2/D_c)$ are suppressed. Furthermore, $\lambda \ll D_c$ is assumed. Particle-hole symmetry is preserved for $\delta_s = 0$ and $\lambda = 0$.

DOS cutoff	General $\bar{V}, \delta_s, \Delta$	Special: $\Delta = 0$
$E_a = E_{20}$	$-D_c - \left(\frac{\bar{V}^2}{D_c} + \frac{\Delta^2}{D_c}\right)$	$-D_c - \frac{\bar{V}^2}{D_c}$
$E_b^- = E_{2\mathbf{Q}}$	$-\frac{1}{2}\left(\frac{\bar{V}^2}{D_c} + \frac{\Delta^2}{D_c}\right) - \frac{1}{2}D_c\left[\left(\frac{\bar{V}^2}{D_c^2}\right)^2 + \frac{\Delta_0^2}{D_c^2} + 2\frac{\Delta_0\delta_s}{D_c^3}\right]^{\frac{1}{2}} + \lambda$	$-\frac{\bar{V}^2}{D_c} + \lambda$
$E_b^+ = E_{30}$	$\frac{1}{2}\left(\frac{\bar{V}^2}{D_c} + \frac{\Delta^2}{D_c}\right) - \frac{1}{2}D_c\left[\left(\frac{\bar{V}^2}{D_c^2}\right)^2 + \frac{\Delta_0^2}{D_c^2} + 2\frac{\Delta_0\delta_s}{D_c^3}\right]^{\frac{1}{2}} + \lambda$	λ
$E_c^- = E_{3\mathbf{Q}}$	$-\frac{1}{2}\left(\frac{\bar{V}^2}{D_c} + \frac{\Delta^2}{D_c}\right) + \frac{1}{2}D_c\left[\left(\frac{\bar{V}^2}{D_c^2}\right)^2 + \frac{\Delta_0^2}{D_c^2} + 2\frac{\Delta_0\delta_s}{D_c^3}\right]^{\frac{1}{2}} + \lambda$	λ
$E_c^+ = E_{10}$	$\frac{1}{2}\left(\frac{\bar{V}^2}{D_c} + \frac{\Delta^2}{D_c}\right) + \frac{1}{2}D_c\left[\left(\frac{\bar{V}^2}{D_c^2}\right)^2 + \frac{\Delta_0^2}{D_c^2} + 2\frac{\Delta_0\delta_s}{D_c^3}\right]^{\frac{1}{2}} + \lambda$	$\frac{\bar{V}^2}{D_c} + \lambda$
$E_d = E_{1\mathbf{Q}}$	$D_c + \left(\frac{\bar{V}^2}{D_c} + \frac{\Delta^2}{D_c}\right)$	$D_c + \frac{\bar{V}^2}{D_c}$

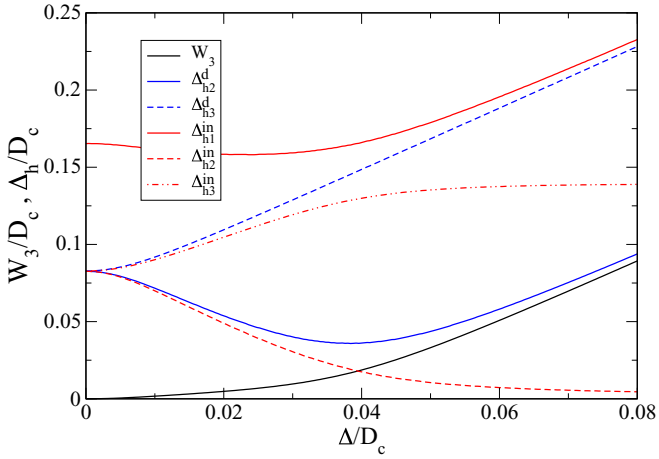

FIG. 4. Hybridization gaps and width of quasiparticle bands $E_{n\mathbf{k}}$ $(n = 1–3)$ (Fig. 2) as function of quasiquartet splitting Δ. Exchange parameters are $J_1^\perp = J_2^\perp = 0.7$ and $J_{12} = 0.1$ with $\mu = -0.081$. Here, $W_3 = E_{3\mathbf{Q}} - E_{30}$ is the central heavy bandwidth (full black line). Direct hybridization gaps are $\Delta^d_{h2} = E_{10} - E_{30}$ (full blue line) and $\Delta^d_{h3} = E_{3\mathbf{Q}} - E_{2\mathbf{Q}}$ (dashed blue line). Indirect hybridization gaps are $\Delta^{in}_{h1} = E_{10} - E_{2\mathbf{Q}}$, the overall indirect gap (full red line), $\Delta^{in}_{h2} = E_{10} - E_{3\mathbf{Q}}$ (dashed red line), and $\Delta^{in}_{h3} = E_{30} - E_{2\mathbf{Q}}$ (dashed-dotted red line). Some gaps behave nonmonotonically as a function of splitting Δ.

Direct hybridization gaps:

$$\Delta^d_{h1} = E_{1\mathbf{Q}'} - E_{2\mathbf{Q}'} = 2(\bar{V}^2 + \Delta^2)^{\frac{1}{2}},$$

$$\Delta^d_{h3} = E_{3\mathbf{Q}} - E_{2\mathbf{Q}} = D_c\left[\left(\frac{\bar{V}^2}{D_c^2}\right)^2 + \frac{\Delta_0^2}{D_c^2}\right]^{\frac{1}{2}} = \left(T^{*2} + \Delta_0^2\right)^{\frac{1}{2}}$$

$$\equiv E_{10} - E_{30} = \Delta^d_{h2}; \tag{18}$$

Indirect hybrization gaps:

$$\Delta^{in}_{h1} = E_{10} - E_{2Q}$$

$$= \left(\frac{\bar{V}^2}{D_c} + \frac{\Delta^2}{D_c}\right) + D_c\left[\left(\frac{\bar{V}^2}{D_c^2}\right)^2 + \frac{\Delta_0^2}{D_c^2}\right]^{\frac{1}{2}}$$

$$\simeq T^* + \left(T^{*2} + \Delta_0^2\right)^{\frac{1}{2}},$$

$$\Delta^{in}_{h3} = E_{30} - E_{2\mathbf{Q}} = \left(\frac{\bar{V}^2}{D_c} + \frac{\Delta^2}{D_c}\right) \simeq T^*$$

$$\equiv E_{10} - E_{3\mathbf{Q}} = \Delta^{in}_{h2}. \tag{19}$$

The first direct gap is also valid for the general case $\bar{V}_1 \neq \bar{V}_2$ $(\delta_s \neq 0)$. For $\Delta \to 0$, $\Delta^d_{h1} \equiv 2\bar{V}$ as in the single-f-orbital KL and $\Delta^d_{h2,3} = T^*$. Thus, in the two-orbital KL there are also *direct* hybridization gaps $\Delta^d_{h2,3}$ which are equal to the Kondo low-energy scale T^*. For the calculation of T^* in terms of the microscopic model parameters, the self-consistency equation (10) under the particle-number constraint for n_f has to be solved. We will do this for general $\bar{V}_1, \bar{V}_2$. Then, due to the lack of spectral symmetry, all three direct as well as indirect hybridization gaps are inequivalent (Fig. 4).

Corresponding to the flat parts of the dispersions we may also introduce effective renormalized quasiparticle masses m_n^* $(n = 1–3)$ in relation to the underlying unhybridized tight-binding model with a band mass $m_b = \frac{\hbar^2 k_F}{D_c}$. We obtain

$$\frac{m^*_{1,2}}{m_b} = \left(\frac{D_c}{\bar{V}}\right)^2 = \frac{D_c}{T^*}, \quad \frac{m^*_3}{m_b} \simeq \left(\frac{\bar{V}}{\Delta}\right)^2 = \frac{T^* D_c}{\Delta^2}, \tag{20}$$

and therefore

$$\frac{m^*_3}{m^*_{1,2}} = \left(\frac{T^*}{\Delta}\right)^2, \tag{21}$$

Thus, in the two-orbital model two types of heavy renormalized quasiparticle masses appear: (i) the $m^*_{1,2}$ effective mass of upper/lower hybridized partly heavy bands which are analogous to the one orbital model; (ii) the type m^*_3 effective mass of the central globally heavy band that appears only in the two-orbital model. The latter depends strongly on Δ; it increases with decreasing CEF splitting and diverges for $\Delta = 0$ leading to a flat unhybridized band. Any small residual quasiparticle interactions beyond the present mean field treatment will then localize these states into a twofold-degenerate unscreened localized spin moment which is naturally expected for the present underscreened case. Thus, the CEF splitting which completely suppresses the underscreening for $\Delta \gg T^*$ is necessary to stabilize the itinerancy of the central quasiparticle band. In fact, its width and mass increase or decrease with increasing Δ, respectively. We give a simple estimate for the localization due to renormalized quasiparticle interaction denoted U^*, assumed positive here. The scale of the latter is estimated from fluctuation expansion beyond mean field solution for the one-orbital Anderson lattice model [34]. In the present Kondo limit, it is equivalent to $U^* = (I_{ex}/D_c)T^*$. The central narrow band will stay itinerant as long as $W_3 \geqslant U^*$. This is approximately the case when $\Delta_0 > (I_{ex}/D_c)T^*$. For much smaller Δ_0, W_3 will shrink rapidly (Fig. 4) and localization to a residual spin $S^* = \frac{1}{2}$ will occur. As mentioned in Sec. II, S^* is weakly coupled to the remaining heavy band states and their coherent Fermi-liquid behavior is preserved. Eventually, the effective intersite interactions in the lattice will lead to magnetic order of residual spins.

V. RENORMALIZED GREEN'S FUNCTIONS AND SPECTRAL FUNCTIONS

The determination of Lagrange parameter λ (the effective f-level position) from the self-consistency equation and chemical potential μ from the particle-number constraint is facilitated by the use of spectral functions. They may be computed from the Green's function matrix (in c, f_1, f_2 orbital space) of the model which is defined by

$$\hat{G}_{\mathbf{k}}(i\omega_n) = (i\omega_n - \hat{h}_{\mathbf{k}})^{-1} = \begin{pmatrix} G_c & A_1 & A_2 \\ A_1 & G_{f1} & B \\ A_2 & B & G_{f2} \end{pmatrix}_{\mathbf{k},i\omega_n}. \tag{22}$$

Each element may be given explicitly or in terms of its bare Green's function element (which is nonzero only for the diagonal) and the renormalized conduction electron Green's function $G_c(i\omega_n)$. Alternatively, the elements may be

presented in explicit form as [using $d_{\mathbf{k}}(i\omega_n)$ from Eq. (12)]

$$\begin{aligned} G_c(i\omega_n) &= \big(i\omega_n - \epsilon_{01}^{\lambda}\big)\big(i\omega_n - \epsilon_{02}^{\lambda}\big)/d_{\mathbf{k}}(i\omega_n), \\ G_{f1}(i\omega_n) &= \big[(i\omega_n - \epsilon_{\mathbf{k}})\big(i\omega_n - \epsilon_{02}^{\lambda}\big) - \bar{V}_2^2\big]/d_{\mathbf{k}}(i\omega_n), \\ G_{f2}(i\omega_n) &= \big[(i\omega_n - \epsilon_{\mathbf{k}})\big(i\omega_n - \epsilon_{01}^{\lambda}\big) - \bar{V}_1^2\big]/d_{\mathbf{k}}(i\omega_n) \end{aligned} \tag{23}$$

for the diagonal part and likewise for the off-diagonal terms:

$$\begin{aligned} A_1(i\omega_n) &= \bar{V}_1\big(i\omega_n - \epsilon_{02}^{\lambda}\big)/d_{\mathbf{k}}(i\omega_n), \\ A_2(i\omega_n) &= \bar{V}_2\big(i\omega_n - \epsilon_{01}^{\lambda}\big)/d_{\mathbf{k}}(i\omega_n), \\ B(i\omega_n) &= \bar{V}_1\bar{V}_2/d_{\mathbf{k}}(i\omega_n). \end{aligned} \tag{24}$$

The latter describe the mixing of orbital dynamics due to the Kondo interaction term. The pole structure of $d_{\mathbf{k}}^{-1}(i\omega_n)$ is determined by the three quasiparticle energies [Eqs. (12) and (13)]. The above form is therefore appropriate when, e.g., one wants to calculate the dynamic magnetic susceptibility or optical conductivity in terms of quasiparticle excitation energies. For the moment we are only interested in the orbitally projected density of states (DOS) functions. For this purpose, the use of explicit quasiparticle bands may be circumvented, as was demonstrated already for the one-orbital KL model [1,9]. In this case, we can employ the following representations of diagonal Green's function elements:

$$\begin{aligned} G_c(i\omega_n) &= G_c^0[i\omega_n - \Sigma_c(i\omega_n)] = \frac{1}{[i\omega_n - \Sigma_c(i\omega_n)] - \epsilon_{\mathbf{k}}}, \\ G_{f\tau}(i\omega_n) &= G_{f\tau}^0(i\omega_n) + \frac{\bar{V}_\tau^2}{\big(i\omega_n - \epsilon_{0\tau}^{\lambda}\big)^2} G_c(i\omega_n), \\ \Sigma_c(i\omega_n) &= \Sigma_\tau \frac{\bar{V}_\tau^2}{i\omega_n - \epsilon_{0\tau}^{\lambda}} \quad (\tau = 1, 2) \end{aligned} \tag{25}$$

where $G_c^0(i\omega_n) = (i\omega_n - \epsilon_{\mathbf{k}})^{-1}$ and $G_{f\tau}^0(i\omega_n) = (i\omega_n - \epsilon_{0\tau}^{\lambda})^{-1}$ are the bare conduction electron and f-electron Green's functions and $\Sigma_c(i\omega_n)$ is the conduction electron self-energy due to the Kondo interaction. The nondiagonal parts may be represented as

$$\begin{aligned} A_\tau(i\omega_n) &= \frac{\bar{V}_\tau}{\big(i\omega_n - \epsilon_{0\tau}^{\lambda}\big)} G_c(i\omega_n), \\ B(i\omega_n) &= \frac{\bar{V}_1\bar{V}_2}{\big(i\omega_n - \epsilon_{01}^{\lambda}\big)\big(i\omega_n - \epsilon_{02}^{\lambda}\big)} G_c(i\omega_n). \end{aligned} \tag{26}$$

Thus, all Green's function elements of Eq. (22) may be expressed by the renormalized conduction electron $G_c(i\omega_n)$ which contains the Kondo interaction effect via $\Sigma_c(i\omega_n)$. Then, all spectral functions and generalized DOS functions can be calculated with

$$\hat{\rho}(i\omega_n) = -\frac{1}{\pi}\mathrm{Im}\frac{1}{N_s}\sum_{\mathbf{k}} \hat{G}(\mathbf{k} i\omega_n)_{i\omega_n \to \omega + i\eta}. \tag{27}$$

Using Eqs. (25) and (26), this can eventually be expressed via the bare conduction electron DOS $\rho_c^0(\omega) = (1/N_s)\Sigma_{\mathbf{k}}\delta(\omega - \epsilon_{\mathbf{k}})$. There are two straightforward model expressions for this quantity:

$$\begin{aligned} &\text{SQ-DOS: } \rho_c^0(\omega) = \frac{1}{2D_c}\Theta_H(D_c - |\omega|), \\ &\text{TB-DOS: } \rho_c^0(\omega) = \left(\frac{4}{\pi^2}\right) K\left(1 - \frac{\omega^2}{D_c^2}\right)\frac{1}{2D_c}\Theta_H(D_c - |\omega|). \end{aligned} \tag{28}$$

The first is a constant square box DOS $\rho_c^0 = 1/2D_c$ within the interval $|\omega| \leqslant D_c$ ($2D_c$ = bare conduction bandwidth). The second possibility corresponds to the DOS of the 2D nearest-neighbor (NN) tight-binding (TB) model also used for the dispersion in Fig. 2, namely, $\epsilon_{\mathbf{k}} = -(D_c/2)(\cos k_x + \cos k_y)$. Due to the (complete) elliptic function $K(x)$ (of the first kind) it has a logarithmic van Hove singularity at $\omega = 0$ ($x = 1$). Then, using Eqs. (25) and (26), all components of Eq. (27) may be expressed by $\rho_c(\omega)$ and $\Sigma_c(\omega)$. One obtains

$$\begin{aligned} \rho_c(\omega) &= \rho_c^0[\omega - \Sigma_c(\omega)], \\ \rho_{f\tau}(\omega) &= \frac{\bar{V}_\tau^2}{\big(\omega - \epsilon_{0\tau}^{\lambda}\big)^2}\rho_c(\omega), \\ \rho_f(\omega) &= \sum_\tau \rho_{f\tau}(\omega), \\ \rho_{A\tau}(\omega) &= \frac{\bar{V}_\tau}{\big(\omega - \epsilon_{0\tau}^{\lambda}\big)}\rho_c(\omega). \end{aligned} \tag{29}$$

For special parameters (e.g., Figs. 2 and 5) the DOS functions may have the spectral symmetries $\rho_{c,f}(\omega) = \rho_{c,f}(-\omega)$ and $\rho_\tau(\omega) = \rho_{\bar{\tau}}(-\omega)$ (see Sec. VII). The partial f-DOS $\rho_{f\tau}$ and "hybridization DOS" $\rho_{A\tau}$ are derived from the renormalized ρ_c by multiplication with (singular) prefactors. Therefore, we first discuss the renormalized conduction electron DOS itself. For the square DOS model of Eq. (28) it is shown in Fig. 5(a). The two hybridization gaps and the central band are clearly visible. The cutoff energies of the bands (DOS and hybridization gap boundaries) are designated in analogy to the single-f-orbital KL model [9]. They are summarized in Table I (see also Fig. 2). The limits in the last column are for $\Delta \to 0$, i.e., the degenerate f quartet. In this case, $E_b^+ = E_c^- = \lambda$ are degenerate because the central $E_{3\mathbf{k}}$ quasiparticle band is dispersionless in agreement with Eqs. (17) ($W_3 = 0$).

The more physically relevant (total) f-DOS is shown in Figs. 5(b) and 5(c), obtained by using Eq. (29) with square-DOS (b) or TB-DOS (c) models, respectively. The typical DOS singularities at the main hybridization gap boundaries E_b^-, E_c^+ are visible for $\bar{V}_1 = \bar{V}_2 = \bar{V}$. They result from the flat portions of the lower/upper hybridized bands $E_{n=1,2}(\mathbf{k})$ in Fig. 2. Furthermore, the overall flat central band $E_3(\mathbf{k})$ produces a strong narrow f-DOS peak around λ whose width is given by Eq. (17). It has mostly contributions from f_1, f_2 states (Fig. 3) which are shown as dashed lines in Figs. 5(b) and 5(c). The according DOS for the alternative TB model (which really corresponds to Figs. 2 and 3) is shown in Fig. 5(c). Because of the van Hove singularity, the DOS of the central band $E_3(\mathbf{k})$ shows additional structure., but essentially the qualitative bandwidths and hybridization gaps are unchanged.

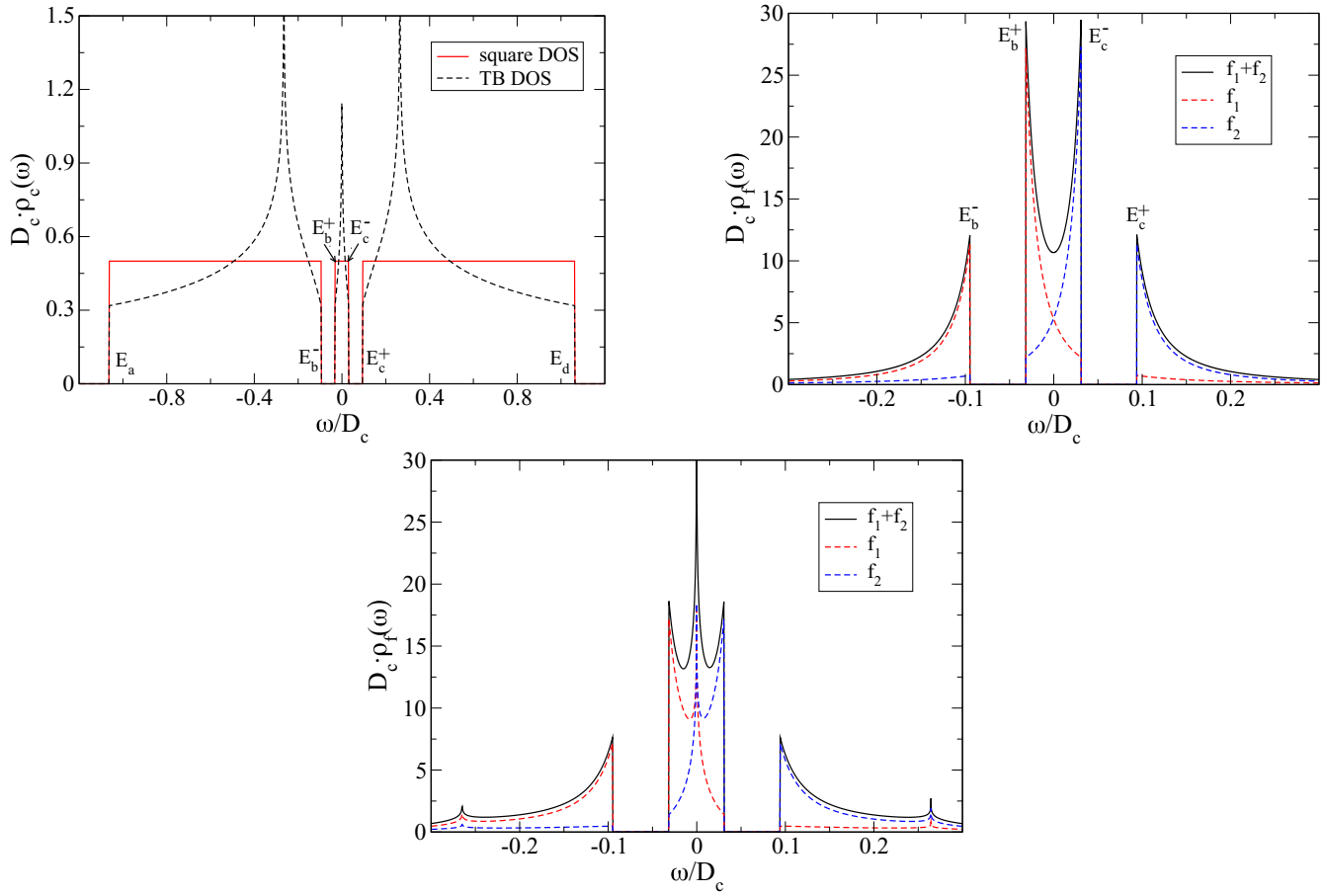

FIG. 5. Renormalized c- and f-DOS for parameters $J_1^\perp = 0.470$, $J_2^\perp = 0.767$, $J_{12} = 0.2$, $\Delta = 0.056$, same as in Fig. 2. Then, the particle-hole-symmetric case is realized with self-consistently determined $\bar{V}_1 = \bar{V}_2 = 0.183$ and setting $\mu = -0.096$, corresponding to $\lambda = 0$. (a) Renormalized conduction electron DOS [Eq. (29)] for square and TB DOS models [Eq. (28)]. (b) Renormalized partial and total f-DOS based on square DOS model of $\rho_c^0(\omega)$. (c) Same quantities based on TB DOS model. (In all figures, the notation a,b,c is from left to right and top to bottom.)

VI. SELF-CONSISTENCY RELATION AND CONSTRAINTS

The DOS functions of Sec. V may be used to express particle-number constraints and self-consistency condition as

$$\begin{aligned} N\int_{-\infty}^{\mu}\rho_c(\omega)d\omega &= n_c,\\ N\int_{-\infty}^{\mu}\rho_f(\omega)d\omega &= n_f \equiv 1,\\ N\int_{-\infty}^{\mu}\rho_{A\tau}(\omega)d\omega &= V_\tau, \end{aligned} \tag{30}$$

where $N = 2$ is the doublet pseudospin degeneracy. These are four equations which determine $\mu, \lambda, \bar{V}_1, \bar{V}_2$ (or V_1, V_2). To gain some insight it is useful to investigate analytical approximate solutions of these implicit equations. For simplicity we use the square DOS model in for $\rho_c^0(\omega)$ in Eq. (28). It has the advantage that the self-consistency equation (10) can be expressed as an algebraic equation and the Kondo scale T^* depends smoothly on μ. We restrict to the symmetric case ($\bar{V}_1 = \bar{V}_2, \lambda = 0$) with $n_c < 1$.

From the first of Eq. (30) one obtains the conduction electron number $n_c(\omega)$. It is shown further below in Fig. 6(a) where it has linear behavior in ω aside from the two small plateaus caused by the hybridization gap $\Delta^d_{h2,3}$ of Eq. (18). Up to the plateau energy we have [$n_c = n_c(\mu)$]

$$\mu = (n_c - 1)D_c - \left(\frac{\bar{V}^2}{D_c} + \frac{\Delta^2}{D_c}\right). \tag{31}$$

For the symmetric case according to Fig. 5(a), $n_c = 1 - W_3/(2D_c)$ holds. For this value of n_c when the conduction states of the lower band are filled Eq. (31) leads indeed, together with Eq. (17), to $\mu = E_b^-$, i.e., the chemical potential is pinned to the upper edge E_b^- of the $E_{2\mathbf{k}}$ band where $n_f(\mu) = 1$ [Figs. 6(a) and 6(b)]. Assuming $\Delta \ll T^*$ we may approximate $n_c = 1 - \Delta^2/(T^* D_c)$. For smaller n_c, the chemical potential drops below the edge ($E_b^- - \mu > 0$) [Figs. 6(a) and 6(b)].

Now, we describe the essential procedure how the value of $\lambda - \mu$ may be approximately obtained from the self-consistency equation [last in Eq. (30)]. It may be written as

$$V_\tau = \frac{N\bar{V}_\tau}{2D_c}\ln\frac{\mu - \lambda - (-1)^\tau\Delta}{E_a - \lambda - (-1)^\tau\Delta} \equiv \frac{N\bar{V}_\tau}{2D_c}F_\tau. \tag{32}$$

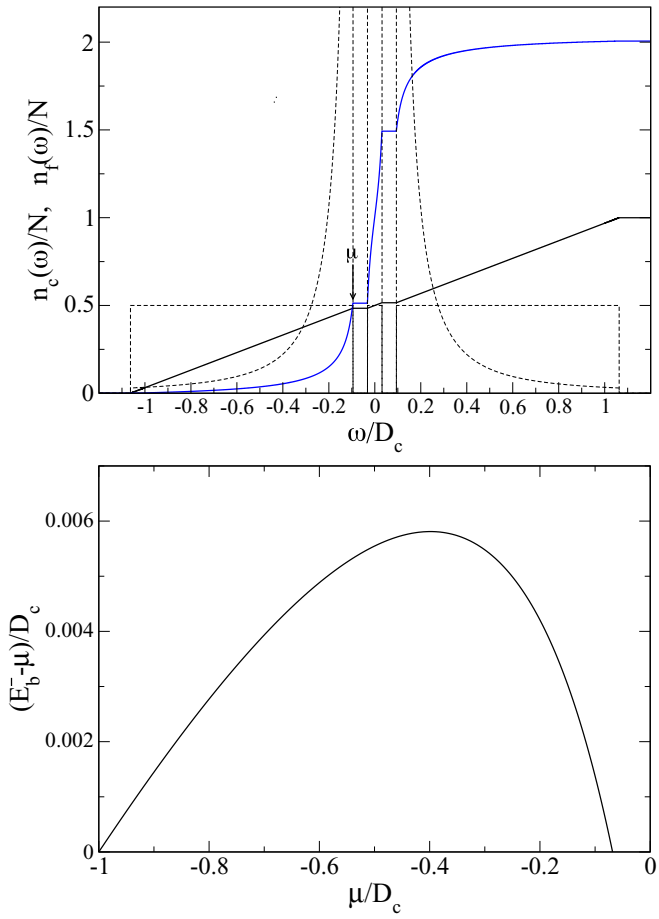

FIG. 6. (a) Integrated conduction and f-electron DOS $n_c(\omega)$ (full black line), $n_f(\omega)$ (full blue line) for the symmetric case (parameters as in Fig. 5). By the constraint the chemical potential $\mu = E_b^-$ lies near the upper edge [see (b)] of lower quasiparticle band such that $n_f(\mu)/N = \frac{1}{2}$. Here, we are also below and close to half-filling $n_c(\mu)/N = \frac{1}{2}$. When μ (or n_c) decreases, the DOS gap structure (dashed lines) is dragged along to lower energy to keep the f occupation $n_f(\mu)/N = \frac{1}{2}$ fixed (see also Fig. 12). (b) Position of chemical potential with respect to upper edge E_b^- of lower band.

Here, we defined the auxiliary function

$$F_\tau(\mu,\lambda) = \int_{-\infty}^{\mu} \frac{\hat{\rho}_c(\omega)}{(\omega - \epsilon_{0\tau}^{\lambda})} \simeq \ln \frac{\lambda - \mu + (-1)^\tau \Delta}{(D_c + \mu) + \lambda - \mu + (-1)^\tau \Delta} \simeq \begin{cases} \ln \frac{\lambda-\mu-\Delta}{Dc} & (\tau = 1), \\ \ln \frac{\lambda-\mu+\Delta}{Dc} & (\tau = 2), \end{cases} \tag{33}$$

where in the first approximation we used $E_a \simeq -D_c$, the second approximation holds for $\lambda, |\mu|, \Delta \ll D_c$. In F_1, F_2 we must have $\lambda - \mu > \Delta$ by definition. Using the transformation given by Eq. (7), we get the matrix self-consistency equation

$$\begin{pmatrix} (N\rho_0)F_1 - \frac{a_1}{A} & -\frac{b}{A} \\ -\frac{b}{A} & (N\rho_0)F_2 - \frac{a_2}{A} \end{pmatrix} \begin{pmatrix} \bar{V}_1 \\ \bar{V}_2 \end{pmatrix} = 0. \tag{34}$$

It implies a relation between the two effective hybridizations given by

$$\bar{V}_1^2 = R\bar{V}_2^2, \quad R = \frac{(N\rho_0)F_2 A - a_1}{(N\rho_0)F_1 A - a_2}, \tag{35}$$

where from now on we use the definitions

$$\begin{aligned} a_\tau &= -\tfrac{1}{2}\big(J_\tau^\perp + \tfrac{1}{2}J_{12}\big), \\ b &= -\tfrac{1}{4}J_{12}, \\ A &= a_1 a_2 - b^2 = \tfrac{1}{4}\big[J_1^\perp J_2^\perp + \tfrac{1}{2}J_{12}(J_1^\perp + J_2^\perp)\big], \\ B &= \tfrac{1}{2}(a_1 + a_2) = -\tfrac{1}{2}\big[\tfrac{1}{2}(J_1^\perp + J_2^\perp) + \tfrac{1}{2}J_{12}\big]. \end{aligned} \tag{36}$$

The solution for $\lambda - \mu$ is then defined by the (secular) self-consistency equation, i.e., the vanishing of the matrix determinant function $F(\lambda - \mu; \Delta)$ given by

$$F(\lambda - \mu, \Delta) = (N\rho_0)^2(a_1 a_2 - b^2)F_1 F_2 - (N\rho_0)(a_1 F_1 + a_2 F_2) + 1 = 0. \tag{37}$$

This is the fundamental equation for the problem which determines $\lambda - \mu$, the effective f-level position above the Fermi energy. It adjusts itself such that the $n_f = 1$ constraint is respected. We may obtain the explicit solution in the simplest special case with $\Delta = 0$, $J_1^\perp = J_2^\perp = J_\perp$, and $J_{12} = 0$ where we get the approximate ($|\mu| \ll D_c$) result

$$T^*(0) := T_0^* = D_c \exp\left(-\frac{2}{g}\right), \quad g = (N\rho_0)J_\perp. \tag{38}$$

Here, T_0^* is the Kondo temperature of each individual doublet since we assumed they are decoupled ($J_{12} = 0$). More general cases are treated in Appendix B. In the most general situation, the self-consistency equation can be solved for $\lambda - \mu$ only numerically. For large Δ it has a unique solution (Fig. 7), for smaller Δ there are two solutions. The larger is the physical one because it corresponds to lower KL ground-state energy and also connects adiabatically to the unique solution for larger Δ [Fig. 7(b)]. To extract the Kondo scale $T^*(\Delta)$ for the general asymmetric case from the numerical solution of Eq. (37) for $\lambda - \mu$ we subtract the effect of Δ on $\lambda - \mu$ [Fig. 7(b)] according to (see also Appendix B)

$$\lambda - \mu = \Delta + T^*(\Delta). \tag{39}$$

Likewise, we may then also compute the effective hybridizations $\bar{V}_\tau$. They are obtained by using $\bar{V}_1^2 = R\bar{V}_2^2$ [Eq. (35)] together with the constraint $n_f = 1$ [Eq. (29)] for the f-electron occupation. The latter may be expressed as

$$n_f = \hat{G}_1 \bar{V}_1^2 + \hat{G}_2 \bar{V}_2^2 = 1. \tag{40}$$

From the two relations we finally obtain

$$\bar{V}_1^2 = \frac{R}{\hat{G}_2 + R\hat{G}_1}, \quad \bar{V}_2^2 = \frac{1}{\hat{G}_2 + R\hat{G}_1}, \tag{41}$$

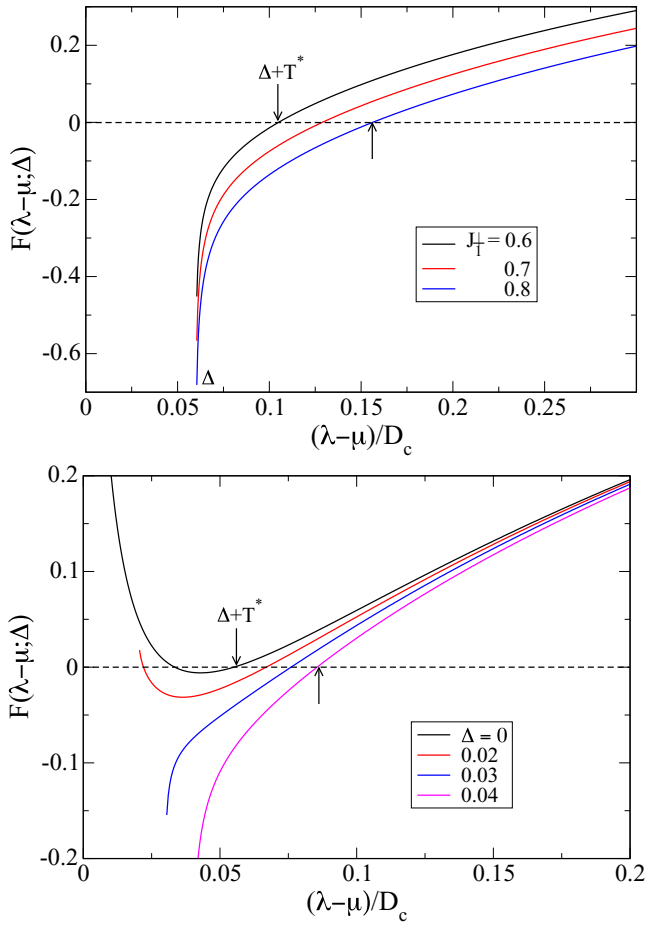

FIG. 7. Self-consistency function $F(\lambda-\mu;\Delta)$. (a) For $\Delta=0.06$, $J_2^\perp=0.6$, $J_{12}=0.1$, and various $J_1^\perp$. (b) For $J_1^\perp=J_2^\perp=0.6$, $J_{12}=0.1$, and various Δ. The intercept with the dashed zero line gives the solution for $\lambda-\mu=\Delta+T^*$. In (b) the lower intercept for small Δ is unphysical (it corresponds to higher ground-state energy).

with R given by Eq. (35). In these expressions we defined $\hat{G}_\tau=(N\rho_0)G_\tau$ with G_τ obtained from

$$\begin{aligned} G_\tau(\mu,\lambda) &= \int_{-\infty}^{\mu}\frac{\hat{\rho}_c(\omega)}{\left(\omega-\epsilon_{0\tau}^{\lambda}\right)^2}d\omega \\ &= \frac{D_c+\mu}{[\lambda-\mu+(-1)^\tau\Delta][(D_c+\mu)+\lambda-\mu+(-1)^\tau\Delta]} \\ &\simeq \begin{cases} \frac{1}{\lambda-\mu-\Delta} & (\tau=1), \\ \frac{1}{\lambda-\mu+\Delta} & (\tau=2), \end{cases} \end{aligned} \tag{42}$$

where again the approximation holds for $\lambda,|\mu|,\Delta\ll D_c$. Without splitting ($\Delta=0$) and equal couplings $J_1^\perp=J_2^\perp$ this leads to $R=1$ and then the symmetric case $\bar{V}_1^2=\bar{V}_2^2$ is realized. In general, for a ratio of $J_2^\perp/J_1^\perp>1$ there is always a value of $\Delta_{cr}>0$ for which the symmetric case occurs (Fig. 8). The original hybridization order parameters V_1, V_2 of Eq. (10) may be obtained from the relation $V_\tau=(N\bar{V}_\tau/2D_c)F_\tau$. With $\lambda-\mu$ and $\bar{V}_\tau$ determined the spectral functions of Eq. (29) with the proper self-consistent energy scales can be determined. As a last step, $n_c(\mu)$ may be

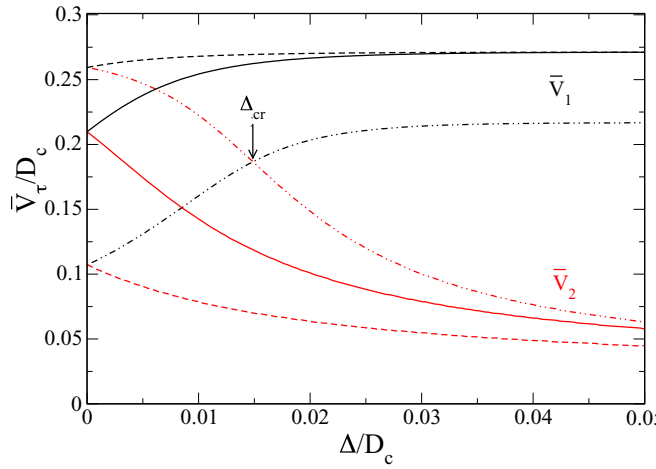

FIG. 8. Self-consistent effective hybridizations $\bar{V}_1$ (black), $\bar{V}_2$ (red) as function of quasiquartet splitting. In all cases, $J_{12}=0.1$. $J_1^\perp=J_2^\perp=0.7$ (full line); $J_1^\perp=0.7$, $J_2^\perp=0.6$ (dashed line); $J_1^\perp=0.6$, $J_2^\perp=0.7$ (dashed-dotted line). In the latter case, the upper level has stronger exchange coupling $J_2^\perp>J_1^\perp$, therefore, there must be a crossing of $\bar{V}_1,\bar{V}_2$ for a special finite Δ_{cr}. For $J_1^\perp=J_2^\perp=0.7$ and $\Delta=0$ (symmetric $\bar{V}_1=\bar{V}_2$ case) we note the agreement of $T^*=\bar{V}^2/D_c\simeq 0.08$ with Fig. 9.

obtained by numerical integration of the first equation in Eq. (30). In order to satisfy the $n_f=1$ constraint, the effective f-level position adjusts itself such that the chemical potential μ always lies close to the upper edge E_b^- of the lower ($n=2$) band for $n_c<1$ as shown in Figs. 6(a) and 6(b).

Finally, we give a closed expression for the ground-state energy in terms of the self-consistently determined λ, order parameters $\bar{V}_\tau$, and auxiliary quantities discussed above. Using Eq. (8) we can write E_{gs}^λ as

$$\begin{aligned} E_{gs}^\lambda/N_s &= (N\rho_0)K_b-\Delta(N\rho_0)\left[\bar{V}_1^2G_1-\bar{V}_2^2G_2\right] \\ &\quad -\tfrac{1}{2}(N\rho_0)^2\left[\left(J_1^\perp+\tfrac{1}{2}J_{12}\right)F_1^2\bar{V}_1^2\right. \\ &\quad \left.+\left(J_2^\perp+\tfrac{1}{2}J_{12}\right)F_2^2\bar{V}_2^2\right] \\ &\quad -\tfrac{1}{2}(N\rho_0)^2J_{12}F_1F_2\bar{V}_1\bar{V}_2. \end{aligned} \tag{43}$$

In the first term we introduced another auxiliary function for the total energy of the renormalized conduction band as given by

$$K_b(\mu)=\int_{-\infty}^{\mu}\hat{\rho}_c(\omega)\omega\,d\omega=\frac{1}{2}\left(\mu^2-E_a^2\right). \tag{44}$$

The ground-state energy of the uncoupled system without exchange terms is obtained as

$$E_{gs0}/N_s=\tfrac{1}{2}\left[\left(N\rho_0^c\right)\left(\mu^2-D_c^2\right)-\Delta\right], \tag{45}$$

and serves as a reference for the (negative) energy gain $\delta E_{gs}(\Delta;\mu)/N_s=(E_{gs}^\lambda-E_{gs0})/N_s$ due to the KL quasiparticle formation. For the most simple case with only the ground state active ($J_2^\perp=J_{12}=0$) we obtain, using $E_a\simeq-(D_c+T^*)$ the result $\delta E_{gs}/N_s=-T^*[1+\ln(D_c/T^*)]$, therefore, the Kondo energy gain is of order T^*.

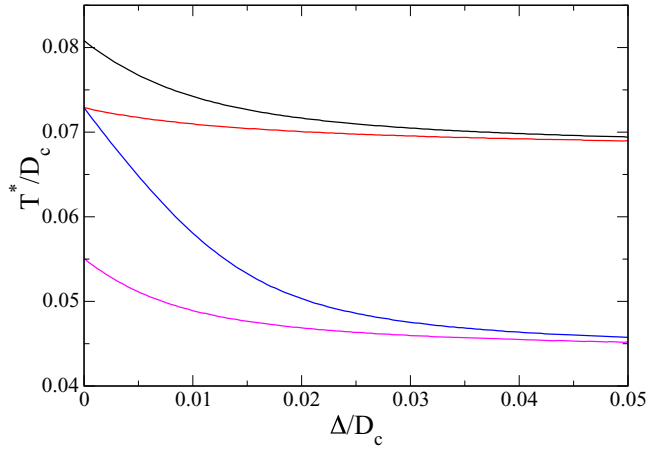

FIG. 9. Kondo energy scale T^* as function of quasiquartet splitting. In all cases $J_{12} = 0.1$. (a) $J_1^\perp = J_2^\perp = 0.7$ (black line); $J_1^\perp = J_2^\perp = 0.6$ (magenta line); $J_1^\perp = 0.7$, $J_2^\perp = 0.6$ (red line); $J_1^\perp = 0.6$, $J_2^\perp = 0.7$ (blue line); the latter two have to be degenerate for $\Delta = 0$.

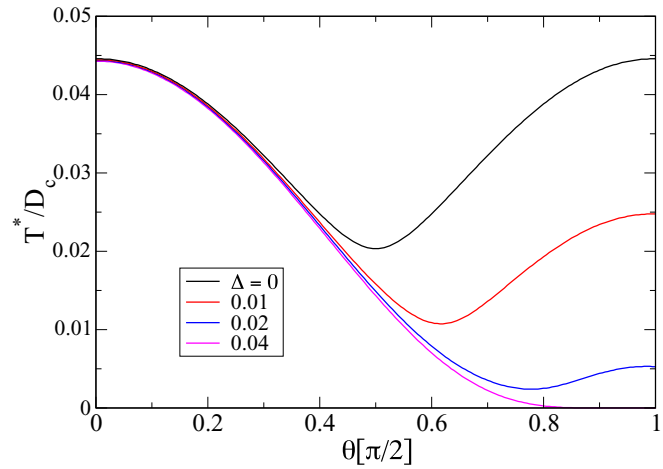

FIG. 10. (a) Variation of T^* with $\theta = \tan^{-1}(J_2^\perp/J_1^\perp)$ for various CEF energies Δ and $J^\perp = 0.6$, $J_{12} = 0.1$ ($J_1^\perp = J_\perp \cos\theta$, $J_2^\perp = J_\perp \sin\theta$). For $\Delta = 0$ due to degenerate upper/lower level the curve is symmetric around $\theta = \frac{\pi}{4}$ or $J_2^\perp = J_1^\perp$. For increasing Δ the influence of the upper level on the Kondo effect is progressively reduced, Therefore, $T^* \to 0$ for $\theta \to \frac{\pi}{2}$, ($J_1^\perp \to 0$).

VII. NUMERICAL SOLUTION FOR THE SELF-CONSISTENCY RELATION AND SPECTRAL FUNCTIONS

The general self-consistency equation (37) has no closed solution for the central quantity $\lambda - \mu$, except in the simplest case $\Delta = 0$ (see Appendix B). Since the dependence of Kondo lattice properties on the quasiquartet splitting is an important issue of this work, we now have to solve it numerically. This means we are looking for the root $\lambda(\Delta) - \mu$ of $F(\lambda - \mu, \Delta) = 0$ [Eq. (37)]. Alternatively, one may solve directly for $T^*(\Delta)$ via the iterative equation (B4). The function $F(\lambda - \mu, \Delta)$ is shown in Fig. 7 for sets of exchange $(J_1^\perp, J_2^\perp, J_{12})$ and fixed Δ [Fig. 7(a)] and for fixed exchange set and various Δ [Fig. 7(b)]. The $(\lambda - \mu)$ position of the zero gives the Kondo scale [Eq. (39)] and determines the self-consistent solution for $\bar{V}_\tau$ using Eq. (41).

The resulting Kondo low-energy scale $T^*(\Delta)$ is shown in Fig. 9 for various exchange parameter sets as function of Δ. As expected, it decreases with increasing quasiquartet splitting because the spin-flip processes (elastic within excited Γ_7 level and inelastic between $\Gamma_6 \leftrightarrow \Gamma_7$) will be suppressed. On the other hand, for the real quartet case $\Delta = 0$ the Kondo scale T^* becomes symmetric with respect to $J_1^\perp$, $J_2^\perp$ [red and blue curves in Fig. 9(a)].

When T^* or likewise $\lambda - \mu$ is known, the effective hybridizations $\bar{V}_\tau$ which determine quasiparticle bands and spectrum can be calculated. It is shown in Fig. 8 for essentially the same parameters as in Fig. 9. Their relative size of $\bar{V}_1$ (black) and $\bar{V}_2$ (red) depends crucially on the order of $J_1^\perp$, $J_2^\perp$. For $J_1^\perp > J_2^\perp$ we naturally have $\bar{V}_1 > \bar{V}_2$ already at $\Delta = 0$ and their difference increases slightly with increasing Δ (dashed lines). For $J_1^\perp = J_2^\perp$ degeneracy at $\Delta = 0$ must occur. But, in both cases for finite Δ we have always $\bar{V}_1 > \bar{V}_2$, which will lead to an asymmetric spectrum as discussed below. The most interesting case is $J_2^\perp > J_1^\perp$, i.e., when the excited Γ_7 has a larger exchange coupling than the ground state Γ_6. Therefore, when $\Delta = 0$ we must also have $\bar{V}_2 > \bar{V}_1$. Because the Kondo effect for the excited state decreases rapidly for increasing Δ so must $\bar{V}_2$, then necessarily a crossing of both curves where $\bar{V}_1 = \bar{V}_2$ at a special value Δ_{cr} that depends on the set $(J_1^\perp, J_2^\perp, J_{12})$. At this value the spectrum may be symmetric for a proper choice of the chemical potential (Fig. 5).

Using these self-consistent values of λ, $\bar{V}_\tau$ we may calculate the quasiparticle bands from Eq. (13), with a special particle-hole-symmetric example given in Fig. 2. Its main heavy band features are characterized by the bandwidths and hybridization gaps given in Sec. IV B. For the general band structure the most important ones are depicted in Fig. 4 as function of Δ. For this case, $J_1^\perp = J_2^\perp$ and the band structure will be asymmetric for $\Delta > 0$. We can clearly see that the bandwidth W_3 of the central $E_{3\mathbf{k}}$ heavy band first increases quadratically and then linearly with Δ compatible with by Eq. (17) (full black line). The evolution of the direct gaps is shown by the red curves and the indirect gaps by blue curves. We observe that one direct and indirect gap show nonmonotonic behavior which is even more pronounced when $J_1^\perp \neq J_2^\perp$. Note that $\Delta_{h2,3}^d$ and $\Delta_{h2,3}^{in}$ are never equal because the particle-hole symmetry is absent for all Δ, however, for $J_2^\perp > J_1^\perp$ they may show a crossing similar to $\bar{V}_1$, $\bar{V}_2$ in Fig. 8.

The exchange parameters $(J_1^\perp J_2^\perp, J_{12})$ of the model are an independent set (Appendix A) that correspond to the CEF parameters. Therefore, one should also know how the low-energy Kondo scale T^* changes with, e.g., the ratio of upper/lower level exchange $J_2^\perp/J_1^\perp$ (Fig. 10). For this purpose we use the polar parametrization $J_1^\perp = J_\perp \cos\theta$, $J_1^\perp = J_\perp \sin\theta$ discussed in the Appendix A. Here, θ varies in the interval $[0, \frac{\pi}{2}]$ corresponding to the change from $J_1^\perp = J^\perp$, $J_2^\perp = 0$ to $J_1^\perp = 0$, $J_2^\perp = J^\perp$. For $\Delta = 0$ upper/lower level are degenerate and therefore $T^*(\theta)$ must be symmetric around $\theta = \frac{\pi}{4}$ or $J_2^\perp = J_1^\perp$. When Δ increases, the upper level contributes progressively less to the effective hybridization and, therefore, together with the complete decoupling of the lower level for $\theta \to \frac{\pi}{2}$, ($J_1^\perp \to 0$) we observe $T^* \to 0$ in Fig. 10. For increasing J_{12} the minimum

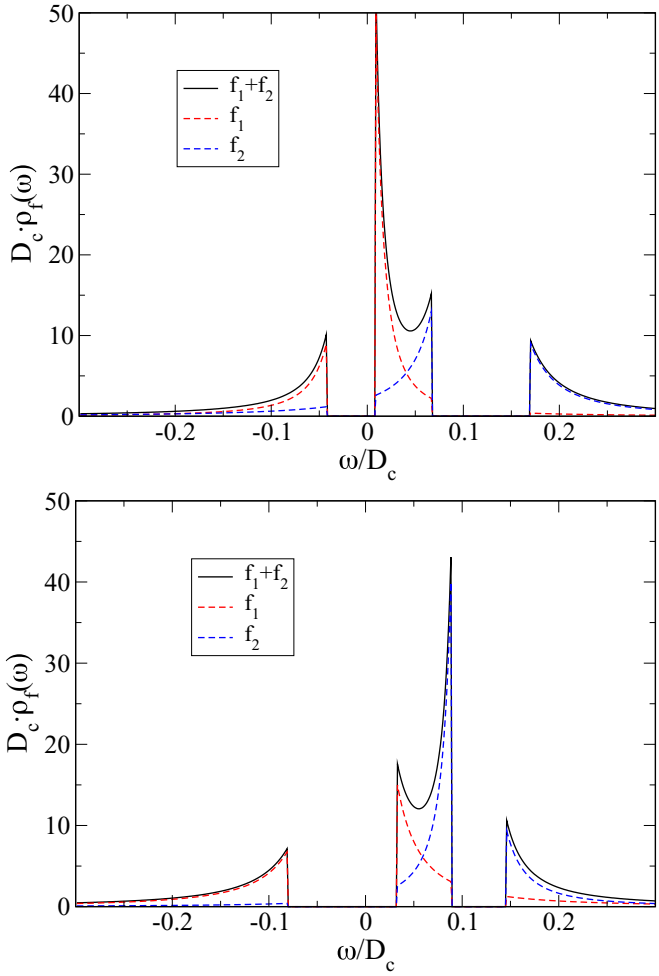

FIG. 11. Renormalized f-DOS of quasiparticles for various asymmetric cases without particle-hole symmetry. (a) $J_1^\perp = 0.4$, $J_2^\perp = 0.8$, $J_{12} = 0.2$, $\Delta = 0.06$, $\mu = -0.04$, (b) $J_1^\perp = 0.6$, $J_2^\perp = 0.8$, $J_{12} = 0.2$, $\Delta = 0.06$, $\mu = -0.08$. When the ratio $J_2^\perp/J_1^\perp$ decreases and Δ grows the central band DOS shifts to larger energies, increasing the left (Δ_{h3}^{in}) and decreasing the right (Δ_{h2}^{in}) hybridization gap. The width of the central band also increases with Δ.

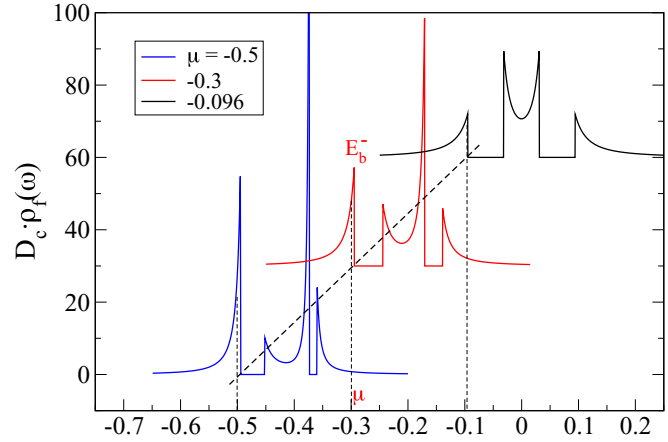

FIG. 12. Evolution of total f-quasiparticle-DOS with chemical potential μ starting from the symmetric case $\mu = -0.096$ ($n_c \simeq 1$) via $\mu = -0.3$ to $\mu = -0.5$ ($n_c \simeq 0.5$). Exchange and CEF parameters like in Figs. 5 and 6. As μ moves to the left, the quasiparticle DOS is dragged along to fulfill the $n_f = 1$ constraint. Therefore, μ is always pinned in the lower f-DOS peak just below E_b^- [connected by thick dashed line, cf. Fig. 6(b)]. The red and black spectra have an ordinate offset of 30 units for clarity.

in $T^*(\theta)$ becomes less pronounced and essentially vanishes for the isotropic case $J_{12} = J_\perp$.

We discussed already basic features of the spectral function in the case that particle-hole symmetry of the original TB band or square DOS model is preserved. This requires special conditions for the self-consistent solution: first we must have $\bar{V}_1 = \bar{V}_2$, i.e., equal effective hybridization strength. This can only be achieved either for $\Delta = 0$ or by fine tuning the CEF energy Δ to a special value Δ_{cr} depending on the exchange parameter set $J_1^\perp$, $J_2^\perp$, J_{12}. For this value, the curves of $\bar{V}_1(\Delta)$ and $\bar{V}_2(\Delta)$ cross (Fig. 8) which is only possible if $J_2^\perp > J_1^\perp$. Furthermore, since the hybridization of bands happens around the effective f-level position λ we must tune $\lambda = 0$ by setting the chemical potential to $\mu = -(\Delta + T^*)$ to achieve the full particle-hole symmetry of quasiparticle bands as depicted in Figs. 2 and 5.

Therefore, the symmetric case requires rather special conditions to be realized. In the case of general size of exchange constants and CEF splitting, the total f spectrum will be quite asymmetric and also the interchange symmetry $f_1 \leftrightarrow f_2$ visible in Fig. 5 will be lost. We present a few characteristic examples for the general case in Fig. 11 (and also Fig. 12) for the underlying square-DOS conduction electron model. In Fig. 11(a) we have $J_2^\perp > J_1^\perp$ and Δ still sufficiently small such that $\bar{V}_2 > \bar{V}_1$. Therefore, the upper hybridization gap will be larger as compared to the lower gap. While the lower and upper bands are still roughly symmetric, the central heavy band is now quite asymmetric because it has shifted out of the center of the overall hybridization gap which would correspond to $\Delta_{h1}^{in} = E_{10} - E_{2\mathbf{Q}}$ in the TB model. In Fig. 11(b) we still have the case $J_2^\perp > J_1^\perp$ but now Δ is sufficiently large to achieve already the inverse relation $\bar{V}_1 > \bar{V}_2$. Therefore, the lower hybridization gap has now become larger than the upper one because the central band is shifted towards the upper band. As a consequence, the skewing of f_1, f_2 distribution is now opposite to that in Fig. 11(a). Thus, by varying Δ or the ratio $J_2^\perp/J_1^\perp$ (i.e., θ), one may shift the central heavy band more or less continuously through the overall hybridization gap and also change its width W_3. For the case $J_1^\perp > J_2^\perp$ we will have $\bar{V}_1 \gg \bar{V}_2$ and therefore the lower hybridization gap dominates while the upper one becomes very narrow. Roughly the upper and central bands have merged into one band separated by a large gap from the lower one. This resembles now the one-orbital case except that the lower and combined upper DOS parts are very asymmetric.

We mostly considered the case for slightly less than half-filling $n_c < 1$. For such case, the chemical potential is pinned very close to the upper edge E_b^- of the lowest band to satisfy the constraint $n_f = 1$ [Fig. 6(a)]. When μ is decreased, one always stays in a metallic situation with the distance $E_b^- - \mu$ behaving nonmonotonically [Fig. 6(b)]. The systematic change of the quasiparticle f-DOS with μ, starting from the symmetric case (close to half-filling $n_c \approx 1$) is presented in Fig. 12. It demonstrates that shifting

the chemical potential to lower values, i.e., reducing the conduction band filling n_c, the hybridized quasiparticle spectrum is dragged along with μ to lower energies such that the chemical potential remains pinned in the DOS peak of the lowest band in accordance with Fig. 6(b). In this way, the f constraint $n_f = 1$ is respected at each band filling n_c.

VIII. CONCLUSION AND OUTLOOK

In this work, we gave a detailed investigation of the quasiparticle spectrum of the underscreened quasiquartet Kondo lattice and the related heavy band structure and associated effective hybridization gaps. A two-orbital model representing Kramers doublets slightly split by a CEF as is frequently found in tetragonal Ce or Yb compounds has been used. We started from an exchange model where f-charge fluctuations are already completely suppressed and single f (electron or hole) occupancy is realized. A fermionic representation of the f conduction electron exchange is employed and the interacting model is treated within a constrained mean field theory that ensures the single f occupancy.

We derived the effective heavy quasiparticle bands and their partial DOS functions. The two-orbital KL model with $N = 2$ degeneracy of conduction band and $2N$ localized states has much richer features than the single-orbital KL model. First, there is in addition a characteristic central heavy band which lies inside the main hybridization gap. It consists mainly of a superposition of the two f states with a small admixture of conduction states that is responsible for the overall dispersion of the central band. The width of this band is itself of the order $W_3 = (T^{*2} + \Delta_0^2)^{\frac{1}{2}} - T^*$ making it a genuinely heavy band of mostly f character. This is in contrast to the upper and lower bands which change their character from light conduction states to heavy hybridized f states and vice versa when traversing the Brillouin zone. Furthermore, due the central heavy band there are now in general three different direct and indirect hybridization gaps, as opposed to just one of each in the single-orbital model. In particular, the two-orbital model has now also a *direct* hybridization gap of the order of the Kondo scale T^*. A rather surprising result is the dependence of the central heavy bandwidth on the CEF splitting Δ. Although the dispersion of the latter is due to the hybridization with c states, it will be nonzero only for finite CEF splitting Δ. In other words, for $\Delta = 0$ the central band will collapse to a flat band which will be localized into a "leftover" spin by residual quasiparticle interactions. This is an inevitable and natural consequence of the underscreened model.

The dependence of T^*, the effective hybridizations $\bar{V}_\tau$, and the associated quasiparticle bandwidth and hybridization gaps on the CEF splitting have been investigated for various parameters of the exchange model. The latter is characterized by two (orbital) diagonal and one off-diagonal exchange constants which are derived from the CEF states. As expected, the increase of Δ decreases T^* due to the reduction of the effective hybridization of the upper doublet when Δ increases. This also explains the reduction of T^* when the ratio $J_2^\perp/J_1^\perp = \tan\theta$ is tuned from small to large values.

The central heavy band in the underscreened KL model is also evident in the various partial DOS spectra. In general, the spectrum is asymmetric with respect to the effective f-level position at λ, i.e., the central band is placed off center in the overall hybridization gap between the lower and upper bands. Also, the distribution of f_1, f_2 orbital weights is asymmetric. This situation prevails for any Δ in the case that $J_2^\perp < J_1^\perp$. In the opposite case $J_2^\perp > J_1^\perp$ there exists a critical Δ_{cr} where the effective hybridizations become equal. Then, with a suitable choice of chemical potential (such that $\lambda = 0$) or n_c the quasiparticle spectrum may become symmetric in energy. In any case, the upper band edge of the lower quasiparticle band must stay pinned to the chemical potential to ensure the single (electron or hole) f occupancy. Then, the central and upper bands must stay unoccupied. This is due to the total suppression of charge fluctuations in the present two-orbital KL model. An analogous Anderson lattice-type model where only the total $n_f + n_c$ occupancy must be preserved allows for c-f charge fluctuations. In this case, with suitable tuning of parameters one could also shift the Fermi level more easily into the central genuinely heavy band. This would also apply to the two-orbital KL model with magnetic polarization.

The interest in this model stems mainly from possible applications to magnetic order in Kondo-lattice compounds. Our detailed investigation of quasiparticle structure lays the foundation for considering this question more realistically than in the canonical but oversimplified one-orbital KL model. For the magnetism, the influence of excited CEF levels in practice always has to be taken into account. We may speculate how to approach it in the framework of the present model theory: In the one-orbital KL model, the true ground state may exhibit ferromagnetic (FM) or antiferromagnetic order, depending on conduction band filling [9,14,35]. In this case, the magnetism appears simply due to the rigid band splitting of hybridized bands into (pseudo)spin-up and -down bands with an ensuing polarization of bands that generates the moment. In the present two-orbital KL model, there is an interesting alternative possibility. Because we have two CEF split f Kramers doublets with a nondiagonal exchange (J_{12}) with conduction electrons, it is possible to develop excitonic (induced) magnetism involving the two orbitals. This may be investigated by either directly breaking the (pseudospin) symmetry and minimize the ground-state energy with respect to the possible magnetic order parameters, as in the one-orbital KL model. Or, one may investigate the magnetic response in the paramagnetic phase to find channels for the instability. Furthermore, one may study the dynamic magnetic response to see whether the magnetism appears via the softening of a mixed CEF/Kondo spin-exciton mode. The detailed investigation of the excitation spectrum in this work provides the solid foundation for such analysis.

ACKNOWLEDGMENTS

A.A. acknowledges financial support through National Research Foundation (NRF) funded by the Ministry of Science of Korea (Grants No. 2015R1C1A1A01052411 and No. 2017R1D1A1B03033465), and by Max Planck POSTECH/KOREA Research Initiative (Grant No. 2011-0031558) programs through NRF funded by the Ministry of Science of Korea.

APPENDIX A: FERMIONIC REPRESENTATION OF THE QUASIQUARTET CEF STATES AND KONDO EXCHANGE MODEL

In this Appendix, we give the schematic derivation of the fermionic representation of Hamiltonian in Eq. (2) from the original Kondo exchange Hamiltonian in Eq. (1). In the latter, the $4f$-charge fluctuations present in the underlying Anderson-type model are already eliminated by a Schrieffer-Wolff transformation [31] for the limit $U_{ff} \gg D_c$ where U_{ff} is the Coulomb repulsion of localized $4f$ states and $2D_c$ the conduction bandwidth. Then, the degrees of freedom are the conduction electrons and CEF split $4f$ states resulting from the spin-orbit ground-state multiplet ($J = \frac{5}{2}$) for $Ce^{3+}(4f^1)$ and ($J = \frac{7}{2}$) for $Yb^{3+}(4f^{13})$ single-electron and hole-type cases, respectively. In a tetragonal environment for, e.g., frequently realized 122 structure of heavy-fermion compounds, the action of the CEF with D_{4h} symmetry splits the $(2J+1)$-fold degenerate $4f$ multiplets into a series of three (Ce) or four (Yb) Kramers doublets belonging to either Γ_6 or Γ_7 representation of D_{4h} (naturally this means that mixed multiple representations must occur). It may happen, in particular in Yb compounds like, e.g., $YbRu_2Ge_2$ [21,22], when the two lowest doublets of Γ_6 and Γ_7 symmetry are close in energy compared to the overall CEF splitting, thus forming a "quasiquartet" state (in cubic symmetry O_h they would combine to a true Γ_8 quartet as for YbB_{12} [19,36] or CeB_6 [6,7]). We focus here on the Yb case when both Γ_6, Γ_7 appear twofold, therefore, their wave functions are linear superpositions of free $4f$ in states $|JM\rangle$ ($|M| \leqslant J$) whose coefficients depend explicitly on the CEF parameters due to the mixing of each pair of representations.

As discussed in Ref. [22], the quasiquartet Γ_6-Γ_7 pair can be represented as

$$\begin{aligned} |\Gamma_6 \pm\rangle &= \alpha_{11}\big|\pm\tfrac{7}{2}\big\rangle + \alpha_{12}\big|\mp\tfrac{1}{2}\big\rangle, \\ |\Gamma_7 \pm\rangle &= \beta_{11}\big|\mp\tfrac{5}{2}\big\rangle + \beta_{12}\big|\pm\tfrac{3}{2}\big\rangle, \end{aligned} \tag{A1}$$

where the pseudospin $\sigma \equiv \sigma_z = \pm 1 (\equiv \pm)$ represents the twofold Kramers degeneracy due to time-reversal invariance. We assume without loss of generality that Γ_6 is the lower and Γ_7 the upper doublet split by an energy Δ_0. The CEF energies may then be defined symmetrically as $E_6 = -\frac{\Delta_0}{2}$ and $E_7 = +\frac{\Delta_0}{2}$. Because the CEF states are those of single $4f$ electrons ($Ce^{3+}, 4f^1$) or holes ($Yb^{3+}, 4f^{13}$) they may be represented as

$$|\Gamma_{6\sigma}\rangle = f^\dagger_{1\sigma}|0\rangle; \quad |\Gamma_{7\sigma}\rangle = f^\dagger_{2\sigma}|0\rangle, \tag{A2}$$

where the "orbital" index $\tau = 1, 2$ corresponds to Γ_6, Γ_7, respectively. Here, $|0\rangle = |f^0, J = 0\rangle$ or $|f^{14}, J = 0\rangle$ is the vacuum or reference state corresponding to the empty or full $4f$ shell from which $f^\dagger_{\tau\sigma}$ creates an electron or hole, respectively. The fermionic representation is then given by

$$H_{\rm CEF} = -\frac{\Delta_0}{2}\sum_{i\sigma}(f^\dagger_{i1\sigma} f_{i1\sigma} - f^\dagger_{i2\sigma} f_{i2\sigma}). \tag{A3}$$

To express the exchange interactions of the Kondo term in fermionic variables, it is also helpful to introduce the pseudospins of the CEF Kramers doublets via the relation [22]

$$S^\alpha_{\tau\tau'} = \frac{1}{2}\sum_{\sigma\sigma'} f^\dagger_{\tau\sigma}\hat\sigma^\alpha_{\sigma\sigma'} f_{\tau'\sigma'}, \tag{A4}$$

where $\hat\sigma^\alpha$ ($\alpha = x, y, z$ or $\pm, z$) are the Pauli matrices for the $S = \frac{1}{2}$ Kramers pseudospins for both orbitals $\tau = 1, 2$. Explicitly, this translates into

$$\begin{aligned} S^z_{\tau\tau} &= \tfrac{1}{2}(f^\dagger_{\tau\uparrow} f_{\tau\uparrow} - f^\dagger_{\tau\downarrow} f_{\tau\downarrow}), \quad S^+_{\tau\tau} = f^\dagger_{\tau\uparrow} f_{\tau\downarrow}, \quad S^-_{\tau\tau} = f^\dagger_{\tau\downarrow} f_{\tau\uparrow}, \\ S^z_{\tau\bar\tau} &= \tfrac{1}{2}(f^\dagger_{\tau\uparrow} f_{\bar\tau\uparrow} - f^\dagger_{\tau\downarrow} f_{\bar\tau\downarrow}), \quad S^+_{\tau\bar\tau} = f^\dagger_{\tau\uparrow} f_{\bar\tau\downarrow}, \quad S^-_{\tau\bar\tau} = f^\dagger_{\tau\downarrow} f_{\bar\tau\uparrow}. \end{aligned} \tag{A5}$$

Here, the pairs $(\tau\bar\tau)$ are defined as either (1,2) or (2,1).

The original Kondo Hamiltonian resulting from the Schrieffer-Wolff transformation comprises all $(2J+1)$ states of the relevant $4f$ multiplet of total angular momentum J. It can be written as [37]

$$\begin{aligned} H_{ex} &= (g_J - 1) I_{ex} \sum_i \mathbf{s}_i \cdot \mathbf{J}_i \\ &= \frac{1}{2}(g_J - 1) I_{ex} \sum_i [J^+_i c^\dagger_{i\downarrow} c_{i\uparrow} \\ &\quad + J^-_i c^\dagger_{i\uparrow} c_{i\downarrow} + J^z_i (c^\dagger_{i\uparrow} c_{i\uparrow} - c^\dagger_{i\downarrow} c_{i\downarrow})], \end{aligned} \tag{A6}$$

where $c^\dagger_{I\sigma}$ creates a conduction electron at lattice site i, J^α_i are the components of the $4f$ total angular momentum operator. Furthermore, I_{ex} is the bare (physical) spin exchange constant (assuming the convention $I_{ex} > 0$ for antiferromagnetic exchange) and g_J the Landé factor to project it to the J multiplet. Since we want to restrict to the lowest two doublets, we can express the J_α operators in this subspace by the pseudospin operators (A4) of these doublets according to

$$\begin{aligned} J^z &= c^z_{11} S^z_{11} + c^z_{22} S^z_{22}, \\ J^\pm &= c_{11} S^\pm_{11} + c_{22} S^\pm_{22} + c_{12}\frac{1}{\sqrt{2}}(S^\pm_{12} + S^\pm_{21}). \end{aligned} \tag{A7}$$

The nondiagonal terms $\sim c_{12}$ are important as they lead to inelastic transitions between the split doublets, thus coupling the Kondo screening of both pseudospins. The linear transformation coefficients may be directly obtained from the CEF wave functions of the original Γ_6, Γ_7 states by the relations

$$\begin{aligned} c^z_{11} &= 7 - 8\alpha^2_{12}, \quad c^z_{22} = -5 + 8\beta^2_{12}, \\ c_{11} &= 4\alpha^2_{12}, \quad c_{22} = 4\sqrt{3}\beta_{12}\sqrt{1-\beta^2_{12}}, \\ c_{12} &= \sqrt{7}\sqrt{(1-\alpha^2_{12})(1-\beta^2_{12})} + \sqrt{30}\alpha_{12}\beta_{12}, \end{aligned} \tag{A8}$$

where the normalization conditions $\alpha^2_{11} + \alpha^2_{12} = 1$ and $\beta^2_{11} + \beta^2_{12} = 1$ have been applied. Using the equivalence of Eq. (A7) and Eqs. (A4) and (A5) in the Hamiltonian of Eq. (A6), we finally arrive at the effective quasiquartet Kondo interaction $H_{ex} = H_{cf} + H^{cf}_{12}$ in Eq. (2). Furthermore, adding the CEF potential of Eq. (A3) and the bare conduction electron part leads to the total model Hamiltonian H of Eq. (2). The interaction constants in this model can then be expressed [22] by the bare sf exchange constant and the coefficients in

Eq. (A8) according to $[J_0 = (g_J - 1)I_{ex}]$

$$J_1^\perp = c_{11} J_0, \quad J_2^\perp = c_{22} J_0, \quad J_{12} = \frac{1}{\sqrt{2}} c_{12} J_0,$$
$$J_1^z = c_{11}^z J_0, \quad J_2^z = c_{22}^z J_0, \quad J_{12}^z = 0. \tag{A9}$$

The vanishing of J_{12}^z is a symmetry property independent of CEF wave-function coefficients. It is obvious from Eq. (A1) since the Γ_6, Γ_7 doublets do not contain $|JM\rangle$ states with equal M. The overall sign of these constants (positive for AF and negative for FM) depends on the sign of the bare spin exchange I_{ex}, the size of g_J, and the sign of CEF derived coefficients in Eq. (A8). In the main text, we will restrict to the case of only positive (antiferromagnetic) effective exchange constants and sometimes use the polar parametrization $J_1^\perp = J_\perp \cos\theta$, $J_1^\perp = J_\perp \sin\theta$ with

$$J_\perp = J_0 \big(c_{11}^2 + c_{22}^2\big)^{\frac{1}{2}}, \quad \tan\theta = \frac{c_{22}}{c_{11}} = \sqrt{3}\frac{\beta_{12}}{\alpha_{12}^2}\sqrt{1-\beta_{12}^2}. \tag{A10}$$

The above relations map the microscopic independent parameters $(J_0, \alpha_{12}, \beta_{12})$ to the independent in-plane exchange model sets $(J_1^\perp, J_2^\perp, J_{12})$ or $(J_\perp, \theta, J_{12})$. The out-of-plane exchange parameter sets (J_1^z, J_2^z) are then fixed by the α_{12}, β_{12} values corresponding to the in-plane set.

The fermionic representation for the exchange model of Eq. (2) has been derived starting from the mapping in Eq. (A2). The latter is possible only for reference (vacuum) states $|0\rangle$ which are fully symmetric such that total angular momentum $J = 0$. This is always the case for Ce^{3+} or Yb^{3+} with reference states corresponding to the empty $(4f^0)$ or full $(4f^{14})$ shell, respectively. Furthermore, it can be used for the nearly half-filled case of Eu^{2+} and Sm^{3+} which also have reference states $(4f^6)$ with $J = 0$ [38,39]. However, for arbitrary occupation of the f shell, the representation of CEF states with Fermi operators is not possible and more general Hubbard or "standard basis" operators [40] with more complicated commutation relations have to be employed.

APPENDIX B: APPROXIMATE EXPRESSION FOR THE LOW-ENERGY SCALE $T^*(\Delta)$

The low-energy scale $T^*(\Delta)$ [Eq. (39)] is determined by the solution of the self-consistency equation (37) which can generally be solved only numerically. In the simplest case ($\Delta = 0$, $J_1 = J_2$, $J_{12} = 0$), $T_0^* = T^*(0)$ reduces to the expression of the Kondo temperature in Eq. (38). We can also give a closed expression of T_0^* for the general exchange model. For $\Delta = 0$ we have $F_1 = F_2 \equiv F_0$ with $F_0 = \ln[(\lambda - \mu)/D_c]$ and then Eq. (37) reduces to

$$(N\rho_0)^2(a_1 a_2 - b^2)F_0^2 - (N\rho_0)(a_1 + a_2)F_0 + 1 = 0. \tag{B1}$$

Using Eq. (36) this self-consistency equation has two possible closed solutions which are given by ($|\mu| \ll D_c$)

$$F_0 = \ln[(\lambda - \mu)/D_c] = -\frac{1}{(N\rho_0^c)\left|\frac{A}{B}\right|}\left[1 \mp \left(1 - \frac{A}{B^2}\right)^{\frac{1}{2}}\right] \equiv -\frac{2}{\tilde{g}_\perp},$$
$$T_0^* = \lambda - \mu = D_c \exp\left(-\frac{2}{\tilde{g}_\perp^0}\right), \tag{B2}$$

where the effective Kondo coupling strength is then given by

$$\tilde{g}_\perp^0 = (N\rho_0^c)\frac{2\left|\frac{A}{B}\right|}{1 - \left(1 - \frac{A}{B^2}\right)^{\frac{1}{2}}} = (N\rho_0^c)\frac{J_{av}^{\perp 2} + \bar{J}_\perp J_{12}}{\left(\bar{J}_\perp + \frac{1}{2}J_{12}\right) - \frac{1}{2}\left[(J_1^\perp - J_2^\perp)^2 + J_{12}^2\right]^{\frac{1}{2}}}. \tag{B3}$$

Here, we defined the two types of orbital-averaged exchange as $J_{av}^\perp = (J_1^\perp J_2^\perp)^{\frac{1}{2}}$ and $\bar{J}_\perp = \frac{1}{2}(J_1^\perp + J_2^\perp)$. Note that of the above two solutions we use only $(-)$ because it has the larger effective coupling $\tilde{g}_\perp$ and hence the largest Kondo energy scale and therefore the lowest ground-state energy. The $(-)$ solution corresponds also to the largest value of $\lambda - \mu$ in the graphical solution plot of Fig. 7(b). In the special case of $J_{12} = 0$ of two decoupled doublets one can show that $\tilde{g}_\perp = \max(J_1^\perp, J_2^\perp)$ and, furthermore, if both are equal then we recover Eq. (38). In the true quartet case ($J_1^\perp = J_2^\perp = J_{12} \equiv J_\perp$) with SU(4) symmetry we obtain $\tilde{g}_\perp = (2N\rho_0^c)J_\perp$ and the corresponding larger Kondo scale T_0^* due to $2N = 4$ degeneracy.

It is also possible to give an approximate closed expression for $T^*(\Delta)$. Using Eq. (39) we may, after some algebra, reformulate the self-consistency in Eq. (37) as

$$T^*(\Delta) = D_c \exp\left(-\frac{2}{\tilde{g}_\perp(T^*, \Delta)}\right)$$
$$-\frac{2}{\tilde{g}_\perp(T^*, \Delta)} = \frac{(N\rho_0)a_2 \ln\frac{D_c}{\Delta_0 + T^*} + 1}{(N\rho_0)^2 A \ln\frac{D_c}{\Delta_0 + T^*} + (N\rho_0)a_1}. \tag{B4}$$

This is still equivalent to Eq. (37). It has the form appropriate for iterative solution for $T^*(\Delta)$. If we stop after the first iteration step, i.e., replacing $T^*(\Delta) \to T_0^*$ at the right-hand side, we get an approximate closed expression

$$T^*(\Delta) = D_c \exp\left[\frac{(N\rho_0)a_2 \ln\frac{D_c}{\Delta_0 + T_0^*} + 1}{(N\rho_0)^2 A \ln\frac{D_c}{\Delta_0 + T_0^*} + (N\rho_0)a_1}\right], \tag{B5}$$

where T_0^* is given by Eqs. (B2) and (B3) and the exchange parameters a_1, a_2, A in Eq. (36). This approximation formula works well when $T^*(\Delta)$ dependence is not too rapid such that the first iteration is sufficient. This is the case for $J_1^\perp \geqslant J_2^\perp$ when the Kondo effect is dominated by the lower doublet and the upper one has moderate influence. For the opposite case $J_2^\perp \geqslant J_1^\perp$, $T^*(\Delta)$ decays rapidly with Δ (see Fig. 9); the approximate formula gives a too rapid decrease with Δ as compared to the numerical solution of Eq. (37) or (B4).

The fundamental quantity in the constrained mean field theory is λ (or $\lambda - \mu$), the position of the effective f level which is adjusted to constrain (on the average) to the Hilbert space with occupation $n_f = 1$. For $\Delta = 0$, the value of $\lambda - \mu$ corresponds directly to the Kondo energy scale T^*. For nonzero Δ the definition of the latter is not unambiguous. One way is to subtract directly the CEF energy according to Eq. (39), another way is to define it as $T^* = \bar{V}^2/D_c$ via the hybridization gaps in the symmetric case as discussed in Sec. IV B. Here, we discuss the connection between the two definitions. Using Eqs. (41) and (42) and assuming T^* from

Eq. (39), we obtain the relation

$$\frac{\bar{V}^2}{D_c} = T^*\left(\frac{1+\frac{\Delta_0}{T^*}}{1+\frac{R}{1+R}\frac{\Delta_0}{T^*}}\right). \tag{B6}$$

In particular, then, for $\Delta = 0$ always $\frac{\bar{V}^2}{D_c} = T_0^*$ as given by Eqs. (B2) and (B3). For the general symmetric case when $\Delta = \Delta_{cr}$ we have $\bar{V}_1 = \bar{V}_2$ or $R = 1$. When $\Delta_{cr}/T^* \ll 1$, the above equation then leads to

$$\frac{\bar{V}^2}{D_c} = T^* + \Delta = \lambda - \mu \tag{B7}$$

consistent with the relation in Eq. (39). In the opposite limit $\Delta_{cr}/T^* \gg 1$, the upper level influence on T^* is negligible and indeed from Eq. (B6) we get $T^* = \frac{\bar{V}_1^2}{D_c}$. Therefore, both definitions of T^* are consistent in the cases where they can be applied simultaneously.

[1] D. M. Newns and N. Read, Adv. Phys. **36**, 799 (1987).
[2] A. C. Hewson, *The Kondo Problem to Heavy Fermions* (Cambridge University Press, Cambridge, 1993).
[3] H. Tsunetsugu, M. Sigrist, and K. Ueda, Rev. Mod. Phys. **69**, 809 (1997).
[4] Y. Kuramoto, *Dynamics of Heavy Electrons* (Clarendon Press, Oxford, 2000).
[5] P. Thalmeier and G. Zwicknagl, in *Handbook on the Physics and Chemistry of Rare Earths* (Elsevier, Amsterdam, 2005), Chap. 219, pp. 135–287.
[6] F. J. Ohkawa, J. Phys. Soc. Jpn. **54**, 3909 (1985).
[7] R. Shiina, H. Shiba, and P. Thalmeier, J. Phys. Soc. Jpn. **66**, 1741 (1997).
[8] M. Sundermann, H. Yavas, K. Chen, D. J. Kim, Z. Fisk, D. Kasinathan, M. W. Haverkort, P. Thalmeier, A. Severing, and L. H. Tjeng, Phys. Rev. Lett. **120**, 016402 (2018).
[9] C. Lacroix and M. Cyrot, Phys. Rev. B **20**, 1969 (1979).
[10] H. Ikeda and K. Miyake, J. Phys. Soc. Jpn. **65**, 1769 (1996).
[11] K. Hanzawa, J. Phys. Soc. Jpn. **71**, 1481 (2002).
[12] V. Y. Irkhin, Phys. Usp. **60**, 747 (2017).
[13] G.-M. Zhang and L. Yu, Phys. Rev. B **62**, 76 (2000).
[14] G.-B. Li, G.-M. Zhang, and L. Yu, Phys. Rev. B **81**, 094420 (2010).
[15] Y. Liu, G.-M. Zhang, and L. Yu, Phys. Rev. B **87**, 134409 (2013).
[16] H. Li, Y. Liu, G.-M. Zhang, and L. Yu, J. Phys.: Condens. Matter **27**, 425601 (2015).
[17] K. S. D. Beach and F. F. Assaad, Phys. Rev. B **77**, 205123 (2008).
[18] S. Hoshino and Y. Kuramoto, Phys. Rev. Lett. **111**, 026401 (2013).
[19] A. Akbari, P. Thalmeier, and P. Fulde, Phys. Rev. Lett. **102**, 106402 (2009).
[20] A. Akbari and P. Thalmeier, Phys. Rev. Lett. **108**, 146403 (2012).
[21] H. S. Jeevan, C. Geibel, and Z. Hossain, Phys. Rev. B **73**, 020407 (2006).
[22] T. Takimoto and P. Thalmeier, Phys. Rev. B **77**, 045105 (2008).
[23] H. S. Jeevan, D. T. Adroja, A. D. Hillier, Z. Hossain, C. Ritter, and C. Geibel, Phys. Rev. B **84**, 184405 (2011).
[24] Z. Huesges, K. Kliemt, C. Krellner, R. Sarkar, H.-H. Klauß, C. Geibel, M. Rotter, P. Novak, J. Kunes, and O. Stockert, New J. Phys. **20**, 073021 (2018).
[25] D. Hafner, B. Rai, J. Banda, K. Klient, C. Krellner, J. Sichelschmidt, E. Morosan, C. Geibel, and M. Brando (unpublished).
[26] T. Saso and H. Harima, J. Phys. Soc. Jpn. **72**, 1131 (2003).
[27] B. Cornut and B. Coqblin, Phys. Rev. B **5**, 4541 (1972).
[28] N. B. Perkins, M. D. Nunez-Regueiro, B. Coqblin, and J. R. Iglesias, Phys. Rev. B **76**, 125101 (2007).
[29] C. Thomas, A. S. da Rosa Simões, J. R. Iglesias, C. Lacroix, N. B. Perkins, and B. Coqblin, Phys. Rev. B **83**, 014415 (2011).
[30] C. Thomas, A. S. da Rosa Simões, C. Lacroix, J. R. Iglesias, and B. Coqblin, J. Magn. Magn. Mater. **372**, 247 (2014).
[31] P. Fazekas, *Lecture Notes on Electron Correlation and Magnetism* (World Scientific, Singapore, 1999).
[32] P. Nozieres and A. Blandin, J. Phys. (Paris) **41**, 193 (1980).
[33] P. Coleman, *Introduction to Many-body Physics* (Cambridge University Press, Cambridge, 2015).
[34] Z. Tesanovic and O. T. Valls, Phys. Rev. B **34**, 1918 (1986).
[35] B. H. Bernhard and C. Lacroix, Phys. Rev. B **92**, 094401 (2015).
[36] P. A. Alekseev, J.-M. Mignot, K. S. Nemkovski, E. V. Nefeodova, N. Y. Shitsevalova, Y. P. Paderno, R. I. Bewley, R. S. Eccleston, E. S. Clementyev, V. N. Lazukov, I. P. Sadikov, and N. N. Tiden, J. Phys.: Condens. Matter **16**, 2631 (2004).
[37] J. Jensen and A. R. Mackintosh, *Rare Earth Magnetism Structures and Excitations* (Clarendon Press, Oxford, 1991).
[38] K. Hanzawa, J. Phys. Soc. Jpn. **67**, 3151 (1998).
[39] T. Takimoto, J. Phys. Soc. Jpn. **80**, 123710 (2011).
[40] M. S. Figueira, M. E. Foglio, and G. G. Martinez, Phys. Rev. B **50**, 17933 (1994).